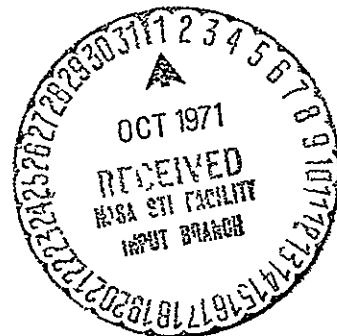
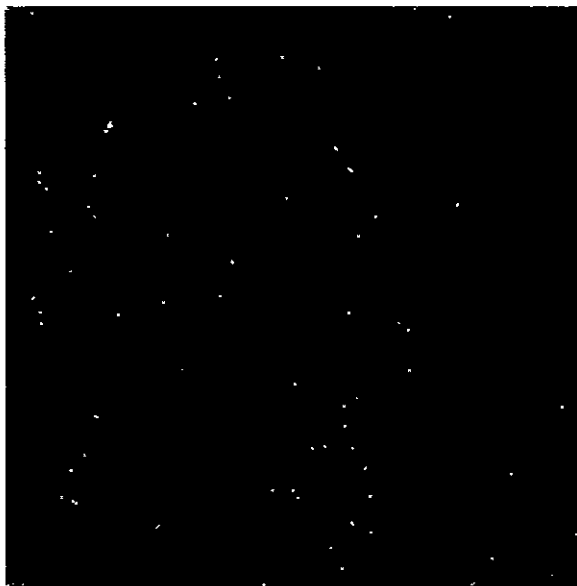


1/14/71



CUBIC CORPORATION

9233 BALBOA AVENUE SAN DIEGO CALIFORNIA 92123

Reproduced by
**NATIONAL TECHNICAL
INFORMATION SERVICE**
U S Department of Commerce
Springfield VA 22151

FACILITY FORM 602

N71-35776	(ACCESSION NUMBER)
103	(PAGES)
CR-115147	(NASA CR OR TMX OR AD NUMBER)
63	(THRU) (CODE)
21	(CATEGORY)

CR-115147



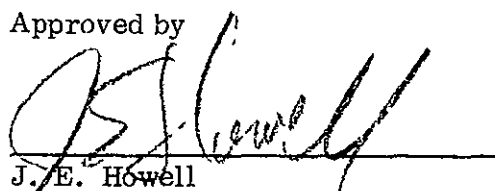
CUBIC
CORPORATION

FTR/16-1

FINAL TECHNICAL REPORT
CR-100 IMPLEMENTATION STUDY
FOR
SPACE SHUTTLE

Prepared for
Intermetrics, Inc
380 Green Street
Cambridge, Massachusetts 02139
under Purchase Order 71-101

Approved by

A handwritten signature in black ink, appearing to read "J. E. Howell", written over a horizontal line.

J. E. Howell
Instrumentation Systems Director



CUBIC
CORPORATION
SAN DIEGO 23 CALIFORNIA

N O T I C E

THIS DOCUMENT HAS BEEN REPRODUCED FROM THE BEST COPY FURNISHED US BY THE SPONSORING AGENCY. ALTHOUGH IT IS RECOGNIZED THAT CERTAIN PORTIONS ARE ILLEGIBLE, IT IS BEING RELEASED IN THE INTEREST OF MAKING AVAILABLE AS MUCH INFORMATION AS POSSIBLE.

CUBIC CORPORATION
San Diego, California

24 June 1971

FOREWORD

This Final Technical Report documents the efforts performed by Cubic Corporation, San Diego, California, for Intermetrics Inc., Cambridge, Massachusetts. This effort was performed under Subcontract Purchase Order 71-101 for Prime Contract NAS 9-11593.

The principal investigator on this Subcontract was Dean G. Krenz, Project Engineer CR-100 Systems, Cubic Corporation, San Diego, California. Others making significant contributions to the program include M. B. Cronkite, Fred Lisenbe and Carl Mehr, all of Cubic Corporation.

CUBIC CORPORATION
San Diego, California

24 June 1971

ABSTRACT

The principal objectives of this program were to examine the performance of the basic CR-100-1 CIRIS designed equipment with respect to the Space Shuttle requirements, and where necessary, to define the product improvements needed to upgrade the equipment to the Space Shuttle requirements. The equipment will be designated Model CR-100-4, Precision Ranging System.

Since the Model CR-100-4 is a modified version of the Model CR-100-1 for CIRIS, a brief functional summary of the CIRIS equipment is presented here.

The CR-100 CIRIS is a Radio Reference Subsystem (RRS) for use with an Inertial Measurement Unit (IMU) in a Completely Integrated Range Instrumentation System (CIRIS). The subsystem consists of an airborne interrogator unit operating under the control of the IMU computer, and one or more ground-based transponders installed at known (surveyed) locations. The RRS design provides a capability for (a) selecting a transponder for interrogation as commanded by the IMU computer, using a digital data link over distances up to 200 miles, (b) measuring the slant range to the transponder with instrumental accuracies to within 3 feet rms, and (c) measuring the range rate of the aircraft with respect to the selected ground station with accuracies to within 0.06 feet per second rms. These accuracies have been demonstrated by actual testing. The IMU computer employs the RRS data to update its own position parameters and thus continually correct for drift.

The performance goal for the Model CR-100-4 is to provide accurate range and velocity information during all phases of Space Shuttle operations including ascent tracking, orbital navigation update, orbital rendezvous, re-entry navigation update, terminal approach and landing.

The measurement accuracy requirement for the Shuttle has been demonstrated in the Model CR-100-1 equipment. The task was to meet the performance goals and still maintain the accuracy. The performance and error analysis shows that 18.5 dB improvement is required in the coherent carrier loop. This improvement is obtained by changing the transmitter and receiver parameters while still retaining the desirable features of a solid state transmitter. The large difference in

Abstract (Continued)

operating ranges required a one step change in transmitter power. The increase in vehicle velocity to 25,500 feet/second requires modification to the acquisition circuitry. Sequential range tones extends the tracking range by a reduction in data loop noise while still retaining the desirable feature of data loop feedback for phase stability. Other modifications are included in Table 1-1, Comparison Summary, CR-100 CIRIS vs CR-100-4 (Space Shuttle).

Analysis shows that the time required for a data sample is about one second in the sub-orbital mode of operation and orbital rendezvous and extends out to 3.7 seconds during orbital navigation update.

The range error model and range rate error model is quite detailed and is summarized in Tables 1-2 and 1-3 for range measurement, and Table 1-4 for range rate measurements. Extensive discussions on the two largest sources of error, namely multipath and propagation effects, are included in the appendixes and under special topics. It is concluded that the maximum practical protection against these sources is included in the design, namely, high modulation index and wide RF bandwidth.

The requirement for a higher power transmitter to protect against signal fade at low elevation angles has been left open ended pending further definition of time requirement during orbital updates. Information on a typical transmitter has been included to perform trade-off studies as the requirements become more defined.

Significant conclusions from the program show that range and range-rate measurements meeting or exceeding the general requirements of the Space Shuttle, can be achieved with only relatively minor electrical modification to the existing Model CR-100-1 design. Producing the equipment will not require development beyond the present "State-of-the-Art" of components and devices.

TABLE OF CONTENTS

I. INTRODUCTION

- A. Purpose of Report
- B. Objectives
- C. Overview
- D. Investigations after Mid-study Report

II. SUMMARY

- A. Comparison CR100-1 CIRIS vs CR100-4 Space Shuttle
- B. Timing Sequence of Events
- C. Range Error Summary
- D. Range Rate Error Summary

III. SPECIAL TOPICS

- A. Amplitude Fade Margin and Ground Antenna Placement
- B. Multipath Effects
- C. Ground Antenna

IV. CONCLUSIONS AND RECOMMENDATIONS

TABLE OF CONTENTS (Continued)

CR-100 Implementation Study for Space Shuttle

1 0	Purpose
2 0	General Requirements
2 1	Operating Frequency
2 2	Maximum Range
2 3	Minimum Range
2 4	Maximum Vehicle Velocity
2 5	Minimum Vehicle Velocity
2 6	Acceleration
2 7	Error Model
2 8	Equipment Constraints
2 9	Acquisition
3 0	Performance and Error Analysis
3.1	Operating Parameters
3 1 1	Frequencies
3 1 2	Dynamic Range
3 1 3	Range Modulation
3 1 4	Dynamics and Drifts
3 2	Coherent Carrier Loop
3 2.1	Minimum IF Bandwidth
3 2 2	Signal-to-Noise Ratio
3 2 3	Carrier Loop Acquisition

TABLE OF CONTENTS (Continued)

3 2 3 1	Orbit Navigation
3 2 3 2	Rendezvous, Re-entry and Landing Navigation
3 2 4	Range Rate (\dot{R}) Data Servo Loop
3 2 4 1	Dynamics
3 2 4 2	\dot{R} Servo Loop Bandwidth
3 2 4 3	Range Rate SNR
3 2 4 4	External Noise Error
3 2 5	Range Rate Counter
3 2 6	Range Data Servo Loop
3 2 6 1	Dynamics
3 2 6 2	Required Loop Bandwidth
3 2 6 3	SNR and Noise Error
3 2 6 4	Lock-up Transient and Settling Time
3 2 6 5	Velocity Error
3 2.7	System Acquisition
3 2 7 1	Data Link
3 2 7 2	Data Link SNR
3 2 7 3	Probability of Error
3 2 7 4	Code Acquisition Time
3 2 8	Calibration
3 2 8 1	Calibration Modes
3 2 8 2	Calibration Accuracy
3 2 9	Drift Considerations

TABLE OF CONTENTS (Continued)

3 2 9 1	Transponders
3 2 9 2	Interrogator
3 2 10	Oscillator Stability
3 2 10 1	Contribution to Range Error
3 2 10 2	Contribution to Range Rate Error
3 2 11	Equipment Noise
3 2 12	Multipath Error
3 2 13	Atmosphere Refractive Index
3 2 14	Range Reference Zero-Crossing Error

APPENDIX A - Effects of Multipath in Distance Measurement
Systems

APPENDIX B - Tropospheric and Ionospheric Propagation
Effects on Range Measurement

APPENDIX C - Tropospheric Propagation Effects on Range Rate
Measurements

APPENDIX D - Section II - Evaluation of SHIRAN Geodetic
Surveying from Flight Test and Evaluation
Program Report.

Technical Report SEG-TDR-64-53

I INTRODUCTION

A Purpose of Report

This report describes the investigations and analysis conducted in developing a precision range (DME) and range rate measuring equipment to perform to the Space Shuttle requirements. The work described in this report was performed by Cubic Corporation under subcontract to Intermetrics, Inc., 380 Green Street, Cambridge, Massachusetts, for Prime Contract NAS 9-11593.

B Objectives

The principal objectives of the investigation and analysis were to examine the performance of the basic CR-100 CIRIS designed equipment with respect to the Space Shuttle requirements, and where necessary to define the product improvements needed to upgrade the equipment to the Space Shuttle requirements.

C Overview

The main body of this report contains the detailed performance and error analysis of the equipment. The summary section below selects the important parameters and differences developed in the main body and presents the results in abbreviated form.

For the reader who is familiar with the Mid-Study Technical Report, ITR/16-1, CR-100 Implementation Study for Space Shuttle, the paragraph "Investigations After the Mid-Study Report" is included to conveniently and quickly acquaint the reader with the new material.

A section on special topics is also added because of the interest generated by the readers of the Mid-Study Report.

D Investigations After the Mid-Study Report

1 It was determined that a range error model was required to adequately describe the performance in the approach and landing phase of operation. Since this phase requires the most accuracy in measurement, this model is a more optimal description of the equipment performance. More information is presented in Paragraph II C.

2 An add-on 60 watt transmitter power module is included to accommodate fade margin discussed in Paragraph II A 2

3 The antenna cable length was considered too short, so the type and length of cable was changed (see Paragraph II A 1)

4 Under Special Topics, multipath, fade margin and ground antenna considerations are discussed in detail because of the high level of reader interest

5 An error was found in Appendix B Tropospheric and Ionospheric Propagation Effects on Range Measurement. In Paragraph II, Case 2, refraction effects for one nautical mile should have been two nautical miles. Complete discussion of the revision is contained in Page 1A of Appendix B.

6. Appendix C Tropospheric Propagation Effects on Range Rate Measurements was found to contain an error. The sign in the second term in the equation for ΔR should have been negative. A complete discussion of the revision is contained in Page 1A of Appendix C

II SUMMARY

A CR-100 CIRIS vs CR-100-4 Space Shuttle

Table 1-1 lists the important parameters and differences developed in the main body under Performance and Error Analysis

The Table has been expanded to include the new concepts since the Mid-Study Report, and the changes and clarifications will be discussed here, leaving the main body of this report unchanged since mid-study.

1 Maximum Range

Item 1 of Table 1-1 lists each contribution to the 18.5 dB signal improvement required to expand the range to 1500 nautical miles. The antenna cable type (Item 1 E) has been changed to allow a greater total length (40 feet) of cable, and still maintain the same signal loss (-1 dB) budget. Cable such as 50-ohm 7/8 in semi-rigid styroflex or spiroline would meet this requirement.

2 Signal Fade Margin

Since signal fade margin may or may not be a requirement (see Paragraph III A), a separate transmitter power module of 60 watts is included for evaluation. This would provide a +7 dB in signal power margin. However, the primary power requirement of over 180 watts just for the module itself, may prohibit its use. The power module is a planar triode amplifier that would be driven by the 12 watt solid state transmitter. A similar amplifier of 100 watts at 1.5 GHz was developed for the Cubic STEER Program. The overall weight of the unit was five pounds including power supply, measuring 4" x 6" x 8".

For further fade margin, the ground antenna pattern can be shaped to provide an additional 2 dB at the desired elevation angle (see Paragraph II C for details).

3 Tracking Range

The tracking range of 1500 nautical miles to 50 feet is beyond the dynamic range of the tracking receiver. Because of this, it is

TABLE 1-1
Comparison Summary, CR-100 CIRIS Vs CR-100-4 (Space Shuttle)

<u>Subsystem Characteristic</u>	<u>CR-100 CIRIS Model</u>	<u>CR-100 Space Shuttle</u>	<u>Space Shuttle Design Improvement</u>
1 Maximum Range	200 miles	1500 N Miles	
A Transmitter Power	4 Watts	12 Watts (solid state)	+5 dB
B Receiver Noise BW	6 kHz	1 kHz	+8 dB
C Data Loop Noise	All Tones	All Tones and/or 1 Tone Sequential	+5 dB
D Noise Figure	7 dB	5 dB	+2 dB
E Antenna Cable Budget	24 Ft (-2 dB)	40 Ft (-1 dB)	+1 dB 7/8" Semi-Rigid Cable
F Frequency	1.6 GHz	2.2 GHz	-2.5 dB
			<hr/> +18.5 dB
2. Signal Fade Margin			
A Transmitter Power Module - - - -		60 watts	+7 dB From 12 watts
B Ground Antenna - - - -		5 dB gain at 10° elevation angle	+2 dB 3 dB has already been allocated on the signal power budget
			<hr/> +9 dB
3 Tracking Range	200 Miles-200 Feet	1500 N Miles - 50 Ft	Requires a one step change in transmitted power Since the transmitter power must be switched, the equipment can track as close in as 3 ft and not exceed receiver dynamic range.
4. Dynamics			
A Velocity	5000 Ft/Sec	25,000 Ft/Sec	(1) Modify sweep acquisition (2) Widen range rate servo loop (3) Increase R counters from 20 bits to 22 bits
B Acceleration	1000 Ft/Sec ²	1000 Ft/Sec ²	Requires no change

Table 1-1 (Continued)

<u>Subsystem Characteristic</u>	<u>CR-100 CIRIS Model</u>	<u>CR-100 Space Shuttle</u>	<u>Space Shuttle Design Improvement</u>
5. Range Modulation Tones			
A Number of Tones	4	5	Extends unambiguous range to 1400 N Miles
B Modes	All tones simultaneous	Simultaneous and sequential	Sequential reduces data loop noise and extends tracking range
6. Sweep rate	One rate	Two rates	(1) Slow rate orbital (2) Fast rate normal Selectable by data link
7. Transmitter	One power level	Two power levels	Low power level for close in range Selectable by data link
8 Data Link			
A Acquisition	8-bit word	8-bit word	Word repeats until system acquisition is complete
B No of Transponders	255	63	Additional capacity is allocated for transmit and sweep functions
C Bit Rate	2500 Bits/Sec	1000 Bits/Sec	Improve SNR at increased range
9. Range Rate Servo	BW = 200 Hz	BW = 500 Hz	Reduce acquisition time in orbital mode
10. Range Servo			
A Fine	BW = 40 Hz	BW = 20 Hz	Improve SNR
B Coarser Tones	BW = 40 Hz	BW = 50 Hz	Decreases settling time for each servo
11. Range Master Oscillator	Stability $1PP 10^6$	Stability $1PP 10^7$	Reduces scale factor error at maximum range

proposed to change the transmitter power level to keep the receiver from saturating. If the power level would be switched as close in as 30,000 feet, the equipment could track in as close as 3 foot range.

B Timing Sequence of Events

Figure 1-1 summarizes the computed times from the main body and presents the results in a timing sequence of events for both the orbital and sub-orbital mode of operation.

C Range Error Summary

1. Orbital

The range errors for the maximum range case are calculated in the main body and summarized in Table 1-2.

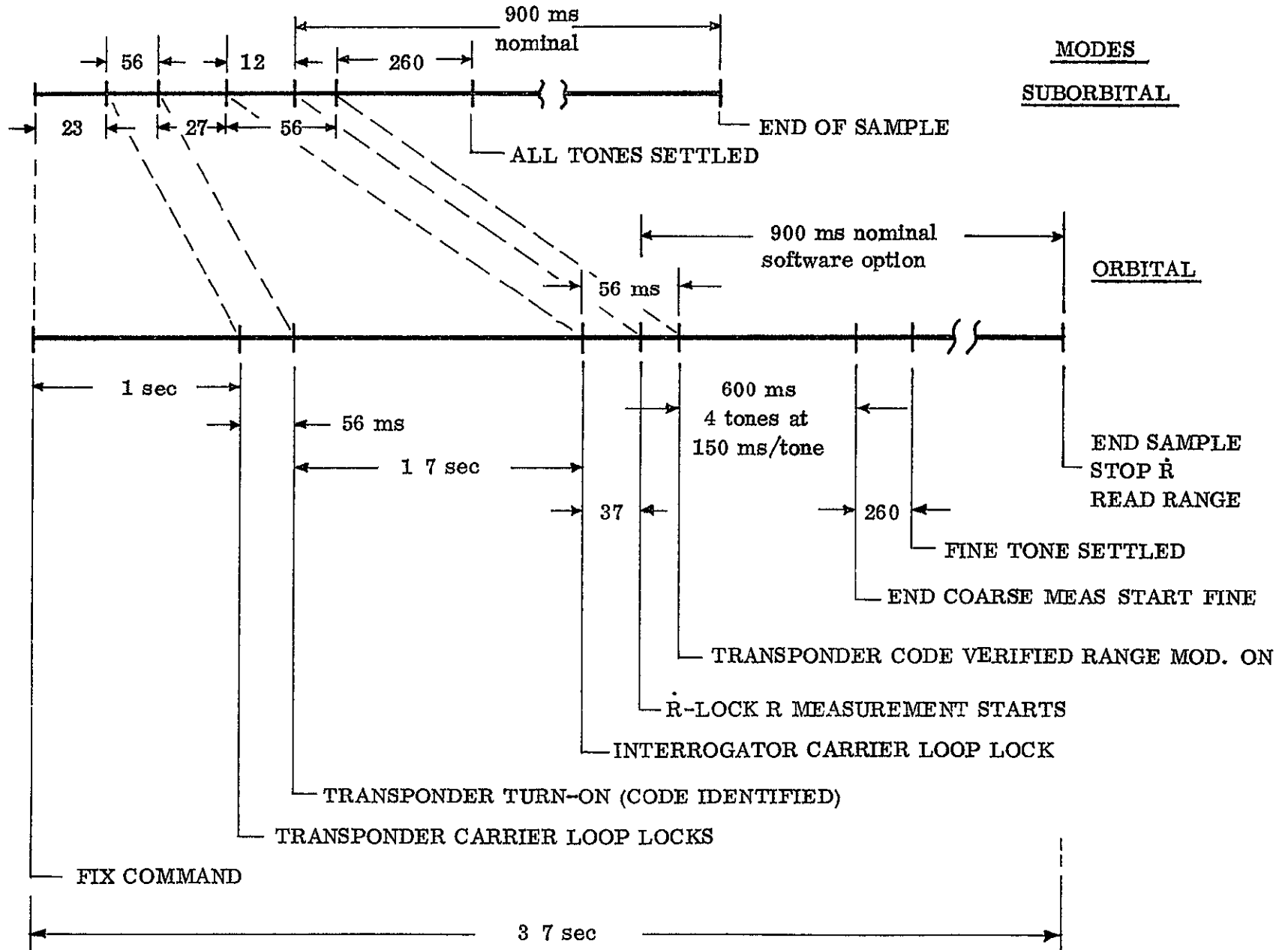
2. Approach and Landing

The approach and landing phase of the shuttle operation is the phase in which the range measurement accuracy requirement is most critical. The inertial measurement unit should have the best possible update information prior to landing. The geometrical placement of the transponders around the landing strip and glide slope path will be such that the slant range and elevation angle from the ground transponder to the interrogator in the shuttle will normally be bounded by 100 meters to 15,000 meters in range and 0° to 90° in elevation angle. Since this is a relatively narrow range of operation for the CR-100-4, it is recommended that the equipment be calibrated and optimized for this phase of operation and allow the range measurement errors at long orbital distances to increase.

The error budget of Table 1-2 is modified and presented in Table 1-3 for this phase of operation. The largest error contribution is from multipath and is explained in detail in Paragraph III B.

The range rate errors are summarized and presented in Table 1-4.

TIMING SEQUENCE OF EVENTS



NOTE UNITS ARE MILLISECONDS UNLESS OTHERWISE LABELED

FIGURE 1-1

CUBIC CORPORATION
San Diego, California

27 April 1971

TABLE 1-2
CR-100 RANGE ERROR BUDGET
MAXIMUM RANGE (ORBITAL MODE)
SPACE SHUTTLE

I. RANDOM ERROR

	Error Source	1 σ Magnitude
A	Ranging error due to finite signal-to-noise ratio and equipment added noise	1 0 ft
B	Phase shift over dynamic range of ranging operations	1 0 ft.
C	Phase shift with temperature over operating environment	1 0 ft
D	Phase shift of interrogator due to vibration, shock and g-loading	negligible
E	System error due to craft dynamics (25,000 ft/sec and 1000 ft/sec ²)	0 2 ft
F	Multipath error in ground-to-air range links	3 0 ft
G	Digitization Error	<u>0 3 ft</u>
	RSS TOTAL	3 5 ft.

II. BIAS ERROR

A	Calibration (Equipment)	1 0 ft.
B.	Scale Factor	
1	Stability of crystal oscillators	0 1 ppm
2	Uncertainty in velocity of light	0 5 ppm
* C	Propagation	
1	N approximation	50.0 ppm
2	End Point Correction	10 0 ppm

* Average - See Appendix B for Error Model

TABLE 1-3
CR-100 RANGE ERROR BUDGET
APPROACH AND LANDING
100 Meters - 15,000 Meters
SPACE SHUTTLE

I	<u>Error Source</u>	<u>1σ Magnitude</u>
	A Ranging error due to finite signal-to-noise ratio and equipment added noise	0.3 ft
	B Phase shift over dynamic range of ranging operations	0.5 ft
	C Phase shift of interrogator due to vibration, shock and g-loading	Negligible
	D System error due to craft dynamics (2,000 ft/sec and 1000 ft/sec)	0.2 ft
	E Multipath error in ground-to-air range links	$3 \cos \phi$ ft
	F Digitization Error	<u>0.3 ft</u>
	RSS TOTAL	$((3 \cos \phi)^2 + (0.7)^2)^{1/2}$
	where ϕ = Elevation Angle	
II	BIAS ERROR	
	A Calibration (Equipment)	. 1.0 ft
	B Phase Shift with Temperature	0.5 ft
	C Scale Factor	
	1 Stability of crystal oscillators	0.1 ppm
	2 Uncertainty in velocity of light	0.5 ppm
	* D Propagation	
	1 N approximation	50.0 ppm
	2 End Point Correction	10.0 ppm

* Average - See Appendix B for Error Model

CUBIC CORPORATION
San Diego, California

27 April 1971

TABLE 1-4

¹ CR-100 RANGE RATE ERROR BUDGET

SPACE SHUTTLE

I VELOCITY INDEPENDENT

	Error Source	1 σ Magnitude
A.	Rate error due to finite signal-to-noise ratio and equipment added noise	.01 ft/sec
B.	System error due to craft dynamics a = 1,000 ft/sec ²	001 ft/sec
C.	Digitization Error	014 ft/sec
D.	Multipath	<u>01 ft/sec</u>
	² RSS TOTAL	02 ft/sec

II. VELOCITY DEPENDENT

A.	Stability of Crystal Oscillator	1 ppm
B.	Uncertainty in Velocity of Light	0.5 ppm
C.	³ Propagation	
	1 N approximation	50.0 ppm
	2 End point correction	10.0 ppm

¹ For $\Delta t = 0.9$ seconds

² Measurement errors under test have been observed at one sigma = .06 ft/sec
This shows some discrepancy between theoretical and actual measurements

³ Average - See Appendix C for Error Model

III SPECIAL TOPICS

A Amplitude Fade Margin and Ground Antenna Placement

Fade margin refers to the signal-to-noise ratio safety factor against fading characteristics of (particularly) fixed ground-to-ground links. Since fading is a statistical property of the signal, it is usually associated with a confidence probability.

According to Bullington ("Radio Propagation Fundamentals," Bell System Technical Journal, Vol 36, No 3, May 1957, pp 600) typical fade margins required for 30-mile line-of-sight paths are

	<u>Confidence Probability</u>		
<u>Frequency</u>	<u>90%</u>	<u>97%</u>	<u>99.9%</u>
4 GHz	6 dB	16 dB	25 dB
1 GHz	5 dB	12 dB	19 dB

Bullington notes that time variations in signal level received over fixed paths are caused by changing atmospheric conditions and that the severity of the fade increases with frequency and path length. He distinguishes between two types (1) inverse bending and (2) multipath effects, the latter including interference between the direct and ground reflected paths and between separate "direct" paths. Inverse bending can decrease the effective path clearance and result in actual obstruction, thus causing slow or long period fading. This type of fading is overcome by having adequate path clearance. Deep fading over water or "smooth" paths results in destructive interference between the direct and reflected paths. This effect is a function of the path length, the carrier frequency, and the antenna heights at the terminals. The effect can be minimized by proper antenna height selection which is always possible for fixed terminals. The third fading phenomena cited by Bullington is that occurring on rough paths with adequate clearance and results in interference between multiple "direct" paths in the atmosphere. Fading due to this mechanization must be accounted for by the link fade margin.

Since the space shuttle operational propagation requirements is not a fixed terminal-to-terminal situation. The carrier fading will be primarily due to multipath fading as the range between the interrogator in the vehicle and the transponder on the ground changes. This is the interference between direct and reflected rays.

Where there is one reflected ray combining with the direct ray at the receiving point (Figure A), the resulting field strength (neglecting the difference in angles of arrival, and assuming perfect reflection at T) is related to the free-space intensity, irrespective of the polarization, by

$$E = 2E_d \sin 2\pi(\delta/2\lambda)$$

where

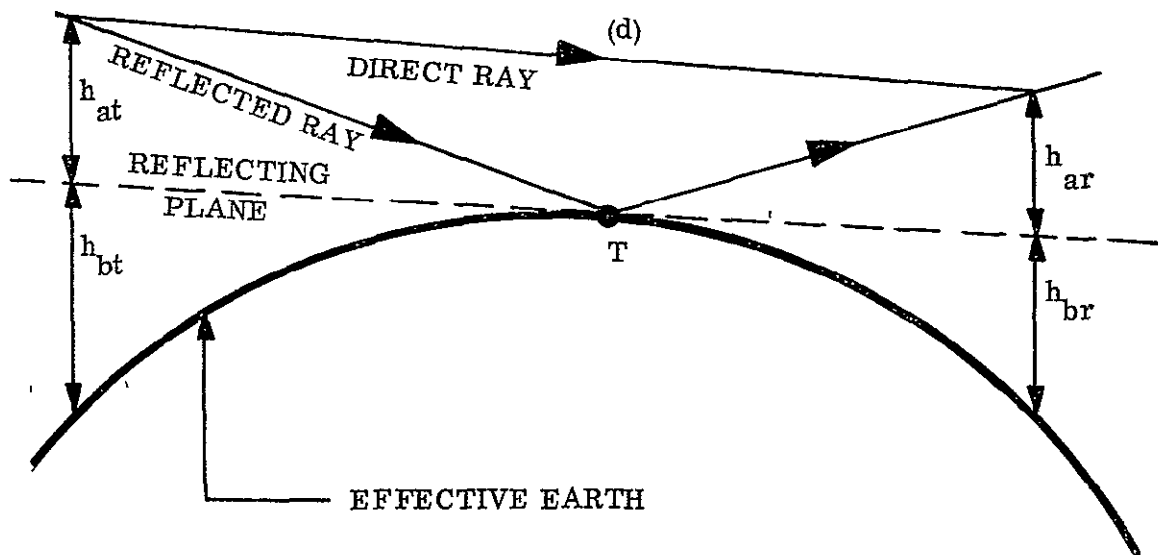
E = resulting field strength

E_d = direct-ray field strength

δ = geometrical length difference between direct and reflected paths,
which is given to a close approximation by

$$\delta = 2h_{at} h_{ar} / d$$

where h_{at} and h_{ar} are the heights of the antennas above a reflecting plane tangent to the effective earth



A--Interference between direct and reflected rays

From the equation, it can be seen that if the geometrical path length difference between the direct and reflected paths is made small, then the variation of field strength with distance will be less sensitive. This can best be accomplished by placement of the ground antenna as close to the ground as possible and still maintain clearance. It should be pointed out that the equation can be used for predicting the frequency of the nulls, but should not be used for the case of the transponder located on the ground, as the equation implies all the signal is reflected from the transponder antenna which is not a true case.

This phenomena was observed during testing of the SHIRAN geodetic survey system developed for the Air Force by Cubic Corporation. Carrier nulls in the order of magnitude of 10 dB to 20 dB were observed at low elevation angles when the transponders were placed on high towers (50 feet). While conducting the flight tests, the transponder height above ground was reduced causing the carrier nulls to move out to greater ranges and become less frequent, thus causing improved operation. One of the tests was conducted with the antenna placed on the ground. No nulls in carrier signal strength were observed, and the aircraft tracked out to distances reduced by only 5% of the distance tracked with the antenna on the high towers. These test results are not presented as all conclusive, as parameters such as the effect of the ground on the antenna pattern was not available. These tests do point out that location of the ground antenna should be given careful consideration for an optimum system.

The space shuttle antenna pattern is also designed to discriminate against multipath below 10° elevation angle (see Figure III-1).

Perhaps the best argument against excessive signal power margin comes from the overall operational system. The signal margin would only be required under conditions of maximum range, low elevation angles and in the orbit-to-earth case. Since the inertial measurement unit and computer predicts the position, signal fade or blanking could be tolerated for short periods of time without serious degradation of position.

B Multipath Effects

The subject of multipath has been of vital interest to the people who are involved in the tracking of the shuttle. For this reason, it was decided to add a paragraph in addition to the brief discussion in the main body, Paragraph 3.2.12 and Appendix A.

CUBIC CORPORATION
San Diego, California

FTR/16-1
Page III-3a

This paragraph adds the experimental work and analysis of flight test results on the SHIRAN Geodetic Survey System. The tests were conducted during Phase III of Contract AF33(657)-7546 that directed a SHIRAN flight test and evaluation program be conducted to demonstrate the system's accuracy in performing all aspects of aerial electronic surveying and controlled photography.

Also included is the rationale for the multipath error term of $3\cos\theta$ ft in the error budget for the approach and landing phase.

Multipath effects are defined as phase and amplitude distortion introduced into the signal path by the presence of the earth and the test vehicle. The literature on the subject is so voluminous that no short discussion can possibly provide a technical review of the field. Multipath effects peculiar to FM transmission have been thoroughly studied since the inception of this modulation technique, and a number of early papers are cited in Sollenberger's paper (Air Force Technical Report No. 12, Ground Reflection Phase Errors of CW-FM Tracking Systems, T. E. Sollenberger) from which much of the work of Appendix A is derived. Similarly, the advantages of high-index FM in suppressing unwanted multipath signals have been fully and adequately documented in the literature. In 1952, Cubic internal document MIS-5 pointed out the advantages of employing high-index FM.

Experimental evidence such as the laboratory and field tests of high-index FM systems, e.g., AERIS, SHIRAN and CLASS, has fully confirmed the suppression predicted by the earlier mathematical investigations.

The SHIRAN overwater tests show the improvement due to increasing the modulation index under actual flight conditions. Section II, Evaluation of SHIRAN Geodetic Surveying of the Flight Test and Evaluation Program Report is included as Appendix D.

A brief description and results of the test is included here for convenience.

The overwater test was performed to check the behavior of SHIRAN over a highly reflective surface and over widely varying geometries. The test consisted of the repeated measurement of a line 184 nautical miles in length at 2000 foot intervals from the minimum altitude of 4500 feet to a maximum altitude of 33,500 feet. The ground station sites selected for the overwater test were stations Point Loma, in the vicinity of San Diego, and Gaviota, in the vicinity of Santa Barbara.

<u>STATION</u>	<u>LONGITUDE</u>	<u>LATITUDE</u>
Gaviota	120° 11' 52.053"	34° 30' 06.542"
Point Loma	117° 14' 27.561"	32° 40' 22.467"

Results of the overwater test showed that lines flown above 12,000 feet demonstrated reasonable internal consistency. The PE_s of these measurements was ± 0.0007 N. Mile with the maximum deviation of -0.0020 N. Mile.

On 20 August 1963, a flight test was conducted for which the modulation index of the SHIRAN equipment was reduced to approximately 5 radians for experimental purposes. At the reduced modulation index, a slight increase in the noise content of the data was noted. This is borne out by the higher residuals and increased probable error. However, the PE_s of the line, ±0.0014 N. Mile, was still within the specification limit. For optimum system performance, all future operations were conducted with a modulation index of approximately 12 radians.

Continuing recognition of high-index spread spectrum techniques for multipath rejection is found in the technical literature. For example, Reed and Blasbalg ("Multipath Tolerant Ranging and Data Transfer Techniques for Air-to-Ground and Ground-to-Air Links," Proceeding of the IEEE, Vol. 58, No. 3, March 1970) state "Thus, if one wants to utilize matched filter detection, the best band-limited signal waveform(s) to use against distributed multipath clutter is one with a flat power spectrum over the bandwidth. Moreover, this waveform and detection process is optimum against a distributed multipath clutter process. The signal-to-clutter can only be improved by increasing the bandwidth which the signal s(t) occupies in accordance with Eq. (19)." Equation 19 is

$$\text{Max (S/N)}_0 = \frac{B \cos \phi}{c \rho E |a|^2}$$

In this equation, B is the receiver bandwidth, $E |a|^2$ is the mean reflection coefficient, ρ is the density of the distributed multipath clutter per unit of distance, c is the electromagnetic wave velocity, and ϕ is the elevation angle of the transmission path.

The intent of this reference is not to derive some theoretical multipath error but to show the dependence of multipath error on receiver bandwidth B, the reflection coefficient $E |a|^2$, the elevation angle ϕ , and couple actual measurement and testing errors as found in ground-to-ground testing (worst case) of the CR-100 equipment. Actual ground-to-ground testing (0° elevation angle) has shown a one sigma error of 3 feet. Flight testing has shown the errors to decrease with elevation angle and minimize at high elevation angle. Literature shows the reflection coefficient as a function of grazing angle to decrease rapidly between 0° and 5°, decline more slowly between 5° and 20°, and slowly rise between 20° and 90° elevation angle with vertically polarized signals. However, the rejection characteristics of the antenna at high elevation angles to multipath reception on the side and back lobes of the antenna virtually eliminates the effects of ground multipath. As a pessimistic error model

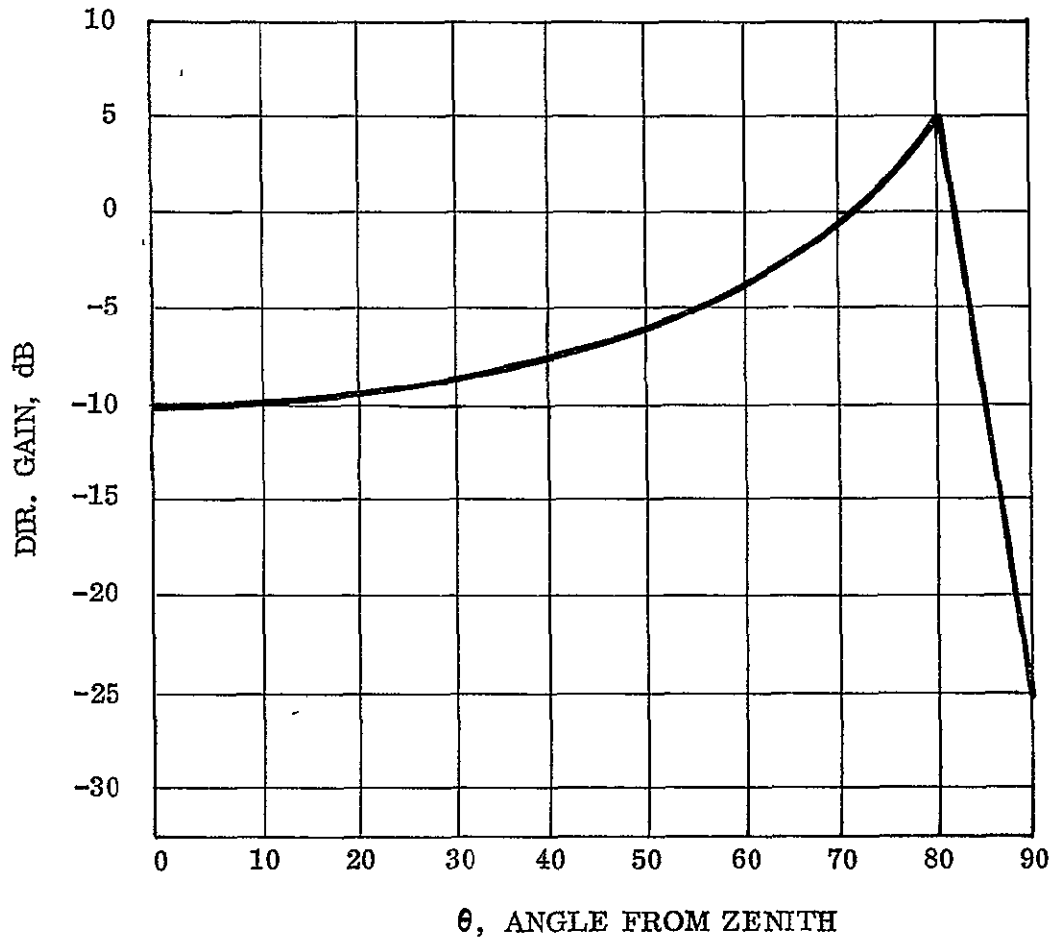


FIGURE III-1 ANTENNA PATTERN REQUIREMENT
FOR SPACE SHUTTLE

for reflection coefficient including antenna side lobe rejection characteristics, one can approximate the reflection coefficient to decrease by the cosine of the elevation angle. From this information is derived the error model of $3 \cos \phi$ ft one sigma where ϕ is the elevation angle. This model does not include the multipath of a specular nature that could arise from poor placement of shuttle antenna next to landing struts, wing-structures and items of this nature.

C. Ground Antenna

The antenna gain required of the space shuttle ground antenna is shown as a function of angle in Figure III-1. This figure is based solely upon the estimated ranges for the space shuttle at various angles. The maximum range of 1500 nautical miles was assumed to occur at an elevation angle of 10° or at an angle of 80° from zenith. The required minimum antenna pattern would be a figure of revolution rotated about $\Theta = 0$.

An antenna which completely satisfies the above requirements is shown in Figure III-2. This antenna consists of a vertically polarized, annular slot contained within a spherical radome-lens. The radome-lens structure is specifically designed to shape the pattern of the annular slot to a pattern which exceeds the levels indicated in Figure III-1. The radome-lens structure not only shapes the antenna pattern, but provides a protective covering for the antenna as well.

The proposed design yields an antenna gain of 5 dB at 80° with a 6 dB design goal. The annular slot antenna described above has been developed by Cubic and used successfully on a number of programs.

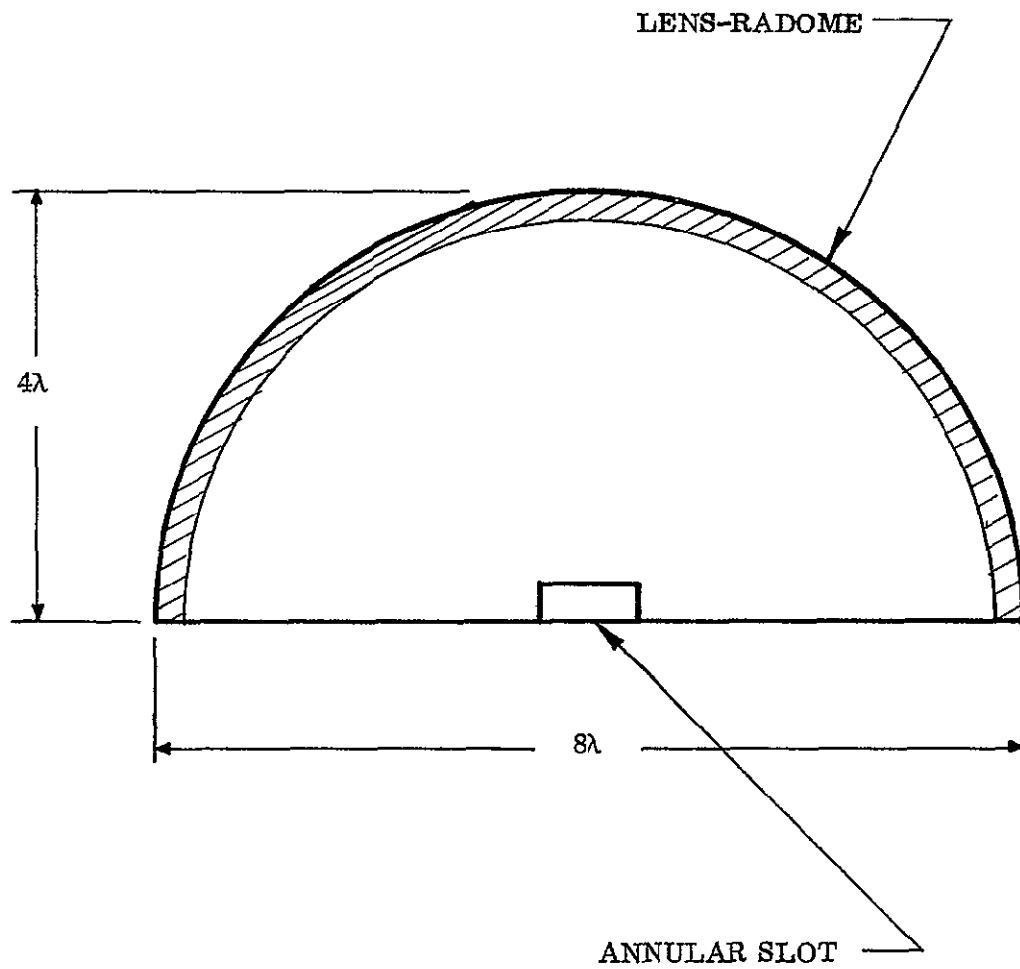


FIGURE III-2 GROUND ANTENNA

IV CONCLUSIONS AND RECOMMENDATIONS

A Conclusions

The demonstrated performance characteristics of the CR-100 equipment and the results of the implementation study show that

1 Range and range-rate measurements meeting or bettering the general requirements of Paragraph 2 0 can be achieved with only relatively minor modifications to the existing CR-100-1 design

2 Producing the equipment will not require development beyond the present "state-of-the-art" of components and devices

B Recommendations

Since the requirement for equipment such as the CR-100-4 is projected to be a reality in only a few short years, it is recommended that a program be started to ensure production of qualified equipment at that time

The program outlined below is a reasonable approach to the problem

PHASE I Procure "carbon" copies of the shorter range CR-100-1 model to perform testing and evaluation of all aspects of lift-off, approach and landing. Problems of integration, antenna patterns, computer programs, astronaut confidence and a host of other potential problems could be solved early in the most cost effective period of time

PHASE II Design, develop and test the changes required to convert the CR-100-1 to the CR-100-4 version. This would run concurrently with Phase I. Build and test the CR-100-4 engineering model, incorporating changes as found in Phase I

PHASE III. Build and space qualify the pre-production units.

PHASE IV Production build of qualified units.

CUBIC CORPORATION
San Diego, California

27 April 1971

CR-100 IMPLEMENTATION

STUDY FOR SPACE SHUTTLE

1 0 PURPOSE

This paper examines the detail requirements of a range and range rate measuring subsystem to meet the space shuttle requirements and where necessary, defines the product improvements needed to upgrade the CR-100 equipment so that it meets these requirements.

2 0 GENERAL REQUIREMENTS

The general requirements and goals of the shuttle mission that affect the electrical properties of the equipment are listed below

2 1 Operating Frequency - S-Band 2.2 GHz

The equipment design calculations will be based on this frequency. Where applicable, the trade off comparisons will be discussed above or below this frequency.

2 2 Maximum Range - 1500 Nautical Miles

Operation beyond this range will be discussed.

2 3 Minimum Range - 50 feet

Operation to within one meter will be discussed.

2 4 Maximum Vehicle Velocity

25,000 ft/sec

2 5 Minimum Vehicle Velocity

0 ft/sec

2.6 Acceleration - 0-1,000 ft/sec²

Operation at landing velocities of 190 knots at 50 ft minimum range will be discussed.

2.7 Error Model - Range - One sigma 4 ft

Range Rate - 0.1 ft/sec.

2.8 Equipment Constraints - Use omni directional antennas

2.9 Acquisition - Sweep Aided

Discuss advantages of computer aided acquisition

3.0 PERFORMANCE AND ERROR ANALYSIS

This paragraph describes the desired performance characteristics, the required parameters, and the predicted errors for the full-limiting, coherent-carrier, range and range-rate measuring subsystem meeting the requirements of Paragraph 2.0. The analysis centers on the interrogator since, with its range and range-rate servo loops, it represents the worst-case condition. However, transponder factors affecting the subsystem are shown wherever relevant.

3.1 Operating Parameters

3.1.1 Frequencies

- A Carrier Frequency Interrogator 2.2 GHz
- B Carrier Frequency Transponder Offset - not relevant for purposes of this study
- C. IF and other frequencies - not relevant for this study

3.1.2 Dynamic Range - 80 dB basic

3.1.3 Range Modulation

Five tones in 250 kHz band

Indexes: 20 for fine tone, 2 for remaining tones

27 April 1971

Data Loop Gain ≈ 30 dB

Data Noise Bandwidth Closed Loop - 750 Hz/tone

Modulation buildup ≈ 10 ms duration

3 1 4 Dynamics and Drifts

Doppler (25,000 ft/sec) ± 113 kHz max Interrogator

± 57 kHz max Transponder

Acceleration (1,000 ft/sec²) ± 4.5 kHz/sec max. Interrogator

Transmitter (TCXO) ± 1 PPM

First LO (TCVCXO) ± 10 PPM

3 2 Coherent Carrier Loop

3.2 1 Minimum IF Bandwidth

Under closed data loop the if index is

$$\text{Index/feedback for fine tone} = \frac{20}{31.6} = 0.64$$

$$\text{for 4 tones} = 4(2/31.6) = 0.25$$

$$\text{Peak deviation} = 0.64 + 0.25 = 0.89$$

and the carrier if. bandwidth B_{if} required by the complex modulating signal is given by

$$B_{if} = 2(\Delta f + 2f_m) + \text{Drifts and Doppler}$$

where, Δf = peak frequency deviation

f_m = highest baseband frequency

$$2 \left[0.89(250 \text{ kHz}) + 2(250 \text{ kHz}) \right] + \text{Drifts and Doppler}$$

$$B_{if} = 2 \left[(250) + 2(250) \right] + \text{Drifts and Doppler}$$

$$B_{if} = 1.446 \text{ MHz} + \text{Drifts and Doppler}$$

27 April 1971

The drifts and doppler affecting the if. bandwidth are calculated as follows

<u>Factor</u>	<u>Interrogator</u>	<u>Transponder</u>
Doppler (25,000 ft/sec.)	±113 kHz	±57 kHz
First LO (10 PPM)	± 22 kHz	±22 kHz
Transmitter (1 PPM)	<u>± 2 kHz</u>	<u>± 2 kHz</u>
Totals	±137 kHz	±81 kHz

Therefore, $B_{if} = 1.446 \text{ MHz} + 0.137 \text{ MHz} = 1.583 \text{ MHz}$

The CIRIS CR-100 is 1.5 MHz which is only a 5% difference in bandwidth.

3.2.2 Signal-to-Noise Ratio (SNR)

The following subparagraphs, Tables and Graphs summarize the important areas within the carrier tracking loop and establishes the basic requirements for the transmitter and receiver in both the Interrogator and the Transponder.

Table 3.1 establishes the received signal power of -125 dBm at maximum range of 1,500 N Miles with 2.2 GHz frequency. A transmitter power output of 12 watts is used and each element in the transmission link is listed in the table. Figures 3.1 and 3.2 are a curve of signal power at the receiver versus range for all operational requirements.

The minimum carrier loop SNR requirements at maximum range with high index single tone range modulation is established at +10 dB for reliable (3-sigma) tracking. Table 3.2 summarizes the important receiver parameters needed to obtain the required SNR at maximum range. Table 3.3 lists the required SNR and receiver sensitivity for all three modes of tracking, i.e., range rate only, range rate and range (1 tone sequential), range rate and range (5 tone simultaneous).

SPACE SHUTTLE CR-100-4
 SIGNAL POWER AT RECEIVER AND SPACE ATTENUATION
 VS
 RANGE (NAUTICAL MILES) FREQUENCY 2.2 GHz

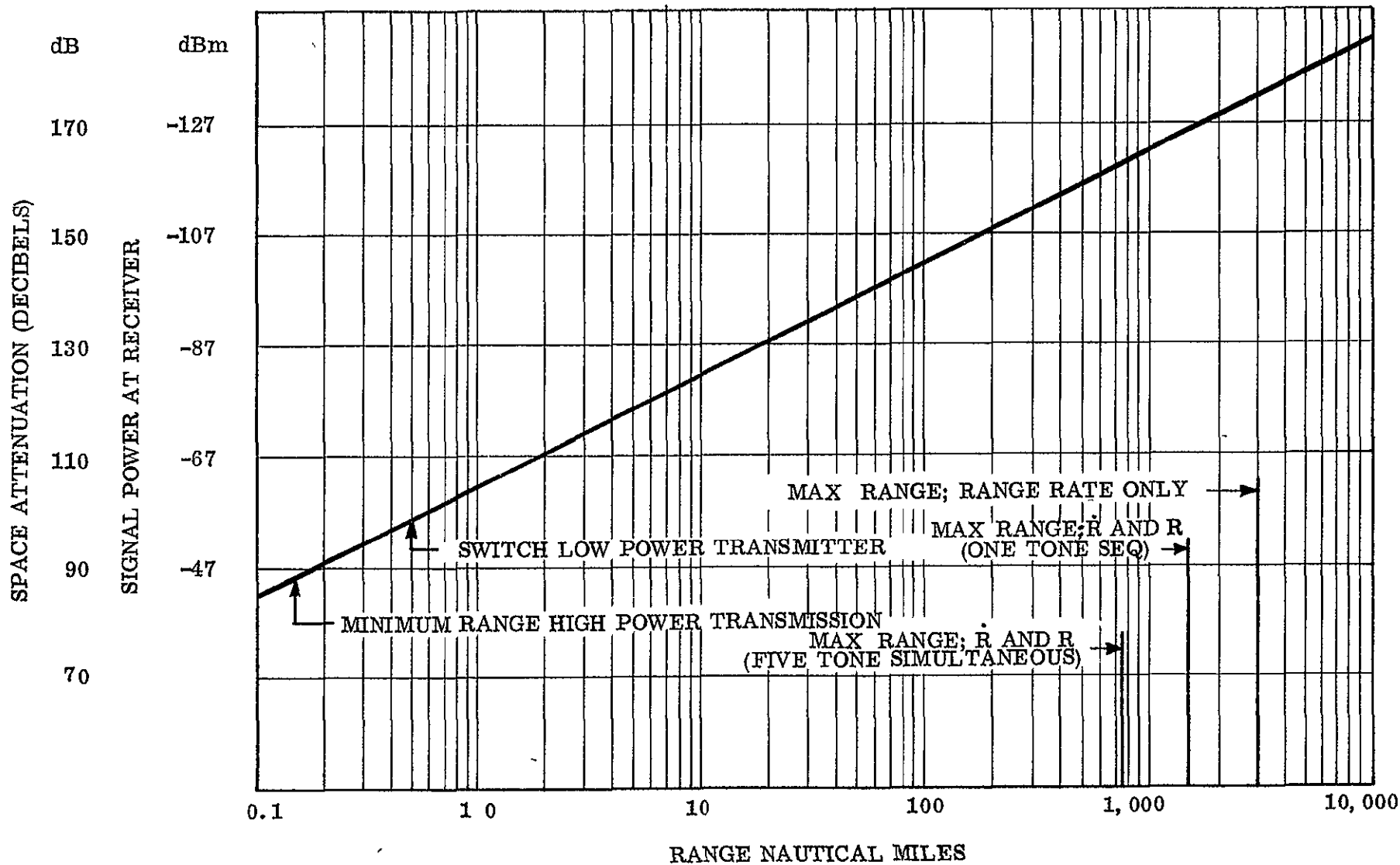


FIGURE 3.1

SPACE SHUTTLE CR100 - 4

SIGNAL POWER AT RECEIVER
VS
RANGE (FEET)
FREQUENCY 2.2 GHz

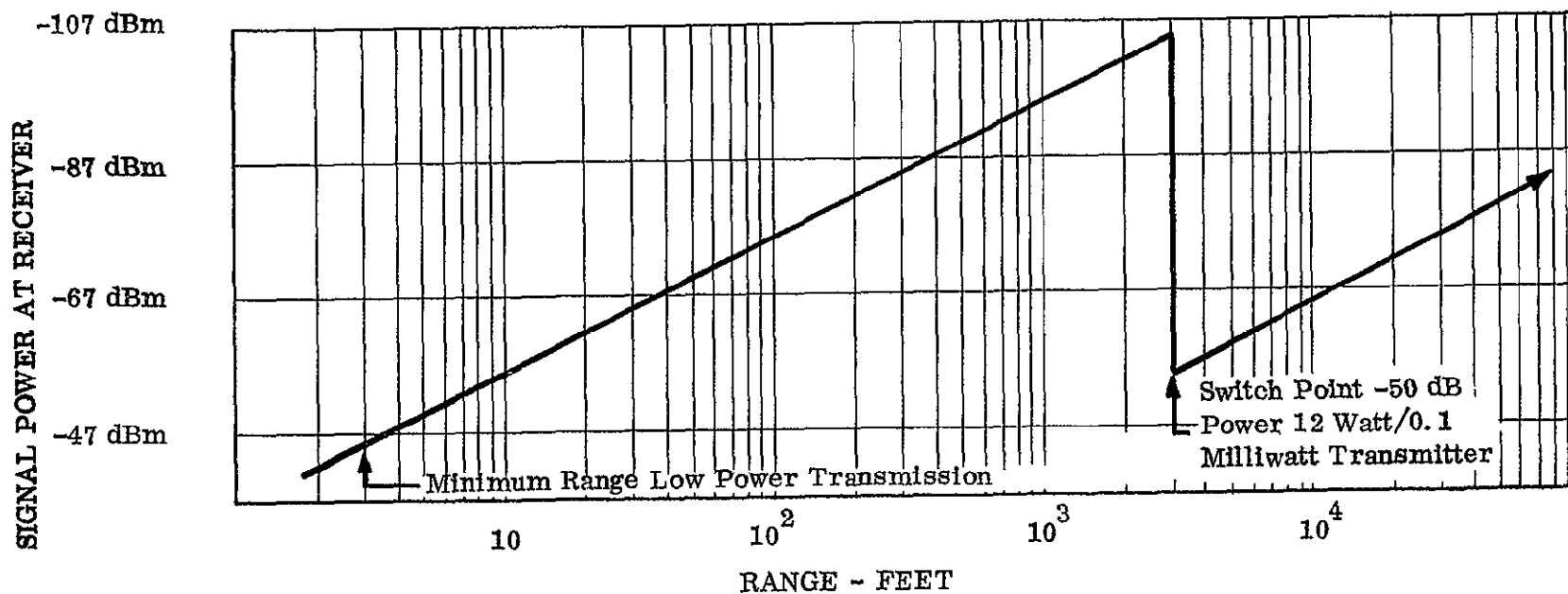


FIGURE 3 2

27 April 1971

TABLE 3.1

Received Signal Power (Maximum Range = 1500 Nautical Miles)

+ 41 dBm	12-watt transmitter output power
<u>- 0.75 dB</u>	Antenna cables transmit path (30 ft 7/8" semi-rigid cable)
+ 40.25 dBm	
<u>0 dB</u>	Antenna gain (Vehicle)
+ 40.25 dBm	
<u>-168 dB</u>	Path attenuation, 1500 Nautical Miles @ 2.2 GHz
-127.25 dBm	
<u>+ 3 dB</u>	Antenna gain (Ground Antenna)
-124.25 dBm	
<u>- 0.25 dB</u>	Antenna cable, receive path (10 ft 7/8" semi-rigid cable)
-125 dBm	Signal power at receiver input

TABLE 3 2

Carrier Loop SNR at 1,500 N Miles

-174 dBm	KTB
5 dB	Noise Figure
62 dB	Noise Bandwidth (11 1 5 MHz)
<u>2 dB</u>	Data Loop Noise Addition (1 tone)
-105 dBm	Noise Power
<u>-125 dBm</u>	Received Signal Power
- 20 dB	
<u>1 dB</u>	Carrier Loss Due to Index (0 64)
- 21 dB	SNR ₁ into the Limiter
<u>1 dB</u>	Loss Due to Limiter
- 22 dB	SNR Out of Limiter
<u>+ 32 dB</u>	Bandwidth Exchange to $2B_L = 1$ kHz
+ 10 dB	Full Modulation at 1,500 N Miles

TABLE 3.3

RECEIVER SENSITIVITY (ALL TRACKING MODES)

	<u>Range Rate Only</u>	<u>Range Rate and Range (1 tone)</u>	<u>Range Rate and Range (5 tones)</u>
KTB	-174 dBm	-174 dBm	-174 dBm
Noise Figure	5 dB	5 dB	5 dB
Loss Due to Limiter	1 dB	1 dB	1 dB
Loss Due to Index	1 dB	1 dB	2 dB
Loss-Data Loop Noise	---	2 dB	7 dB
Bandwidth Exchange (1 kHz)	30 dB	30 dB	30 dB
Required SNR	<u>6 dB</u>	<u>10 dB</u>	<u>10 dB</u>
Receiver Sensitivity	-131 dBm	-125 dBm	-119 dBm

3 2.3 Carrier Loop Acquisition

3 2.3.1 Orbit Navigation

From the signal-to-noise budget at 1,500 N Miles, Paragraph 3.2 2, it is seen that the carrier loop noise bandwidth must be at least 1 kHz at threshold to provide enough SNR for reliable loop lock using high index single range tone modulation on the carrier. This is rather a simple modification from the CIRIS equipment which has a 6 kHz bandwidth. However, the acquisition lockup time now increases.

Since the doppler and drifts are outside the bandwidth of the loop, sweep aided acquisition is used similar to CIRIS. To insure greater than 99% probability of lock during the first sweep, a sweep rate of $\Delta \dot{\omega} = \omega_n^2/2$ (1/2 the theoretical limit) is reasonable,

where ω_n = loop natural frequency

ω_n is a function of the loop noise bandwidth and loop damping factor ζ and is expressed by

$$\omega_n = 2B_L / (\zeta + \frac{1}{4\zeta})$$

where $2B_L = 1,000$ Hz (noise bandwidth)

The sweep rate, therefore, is

$$\Delta \dot{\omega} = \frac{\omega_n^2}{2} = \frac{10^6}{2} \text{ rad/sec}^2$$

or sweep frequency $\Delta \dot{f}$ is

$$\Delta \dot{f} = \frac{\Delta \dot{\omega}}{2\pi} = \frac{10^6}{4\pi} = 80 \text{ kHz/sec.}$$

27 April 1971

The maximum time (T_L) to lock is proportional to the uncertainty of the frequency caused by doppler and drifts. For the Interrogator, the uncertainty is ± 137 kHz at maximum doppler and

$$\text{Max. } T_L = \frac{2(137 \text{ kHz})}{80 \text{ kHz/sec}} = 3.4 \text{ sec.}$$

Average acquisition time is $3.4/2 = 1.7$ sec.

The maximum time (T_L) to lock for the transponder is

$$\text{Max. } T_L = \frac{2(81)}{80} = 2 \text{ sec}$$

and average time is 1 sec.

3.2.3.2 Rendezvous, Re-entry and Landing Navigation

In all categories of tracking, less than 200 N Miles, there is no requirement for the long time sweep acquisition as the relative velocities between Interrogator and Transponder has decreased to less than 2,000 feet/second. Under these conditions, the drifts and doppler is calculated as follows

<u>Factor</u>	<u>Interrogator</u>	<u>Transponder</u>
Doppler (2,000 ft/sec)	± 10 kHz	± 5 kHz
First LO (10 PPM)	± 22 kHz	± 22 kHz
Transmitter (1 PPM)	<u>± 2 kHz</u>	<u>± 2 kHz</u>
Totals	± 34 kHz	± 29 kHz

At this range the power input to the receiver has increased to -107 dBm increasing the SNR into the Limiter to -1 dB. This raises the signal suppression factor (α) and widens the loop bandwidth to $B_L = 1.8$ kHz.

The loop bandwidth is calculated from the formula

$$B_L = B_{LT} \frac{[\alpha/\alpha_T + (4\zeta_T^2)^{-1}]}{[1 + (4\zeta_T^2)^{-1}]}$$

where

$$B_{LT} = 500 \text{ Hz} \quad \text{Loop bandwidth at threshold}$$

$$\zeta_T = 0.5 \quad \text{Damping factor at threshold}$$

$$\alpha_T = 0.99 \quad \text{Limited signal suppression factor at threshold}$$

$$\alpha_{-1 \text{ dB}} = .620$$

$$\alpha = \left(\frac{(\text{SNR})_1}{4/\pi + (\text{SNR})_1} \right)^{1/2}$$

Figure 3.3 plots the loop bandwidth as a function of range and shows the B_L widens out to 2.8 kHz maximum.

The loop damping factor also increases with SNR and is proportional to $\sqrt{\alpha}$ or $\zeta = 1.2$ at $B_L = 2.8$ kHz.

The maximum time to lock can now be calculated.

$$\omega_n = 2B_L / \left(\zeta + \frac{1}{4\zeta} \right) = \frac{2(2800)}{1.4} = 4,000$$

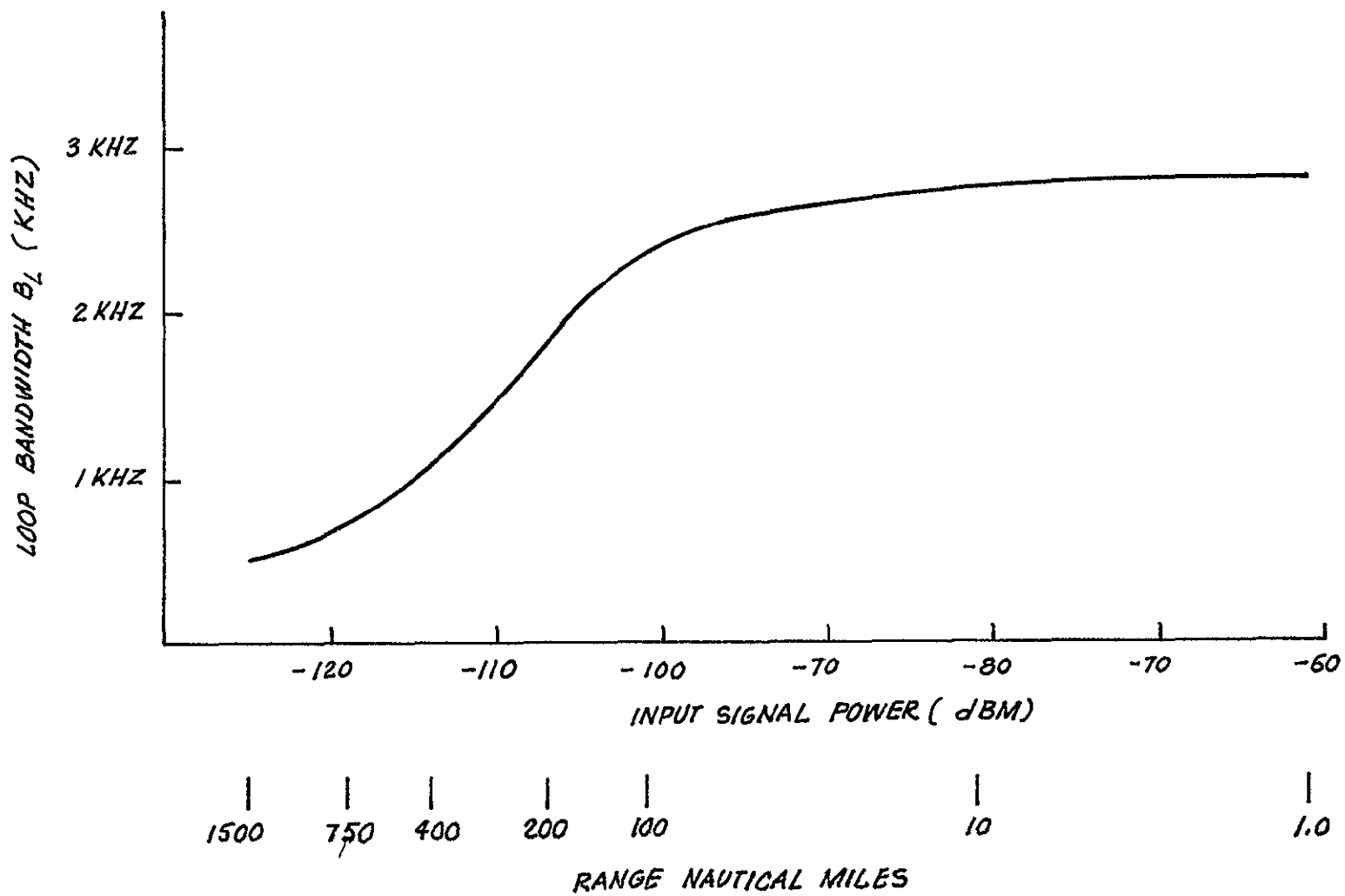
The sweep rate, therefore, is

$$\Delta\omega = \frac{\omega_n^2}{2} = \frac{16 \times 10^6}{2} \text{ rad/sec}^2$$

or sweep frequency Δf is

$$\Delta f = \frac{\Delta\omega}{2\pi} = \frac{16 \times 10^6}{4\pi} = 1.27 \times 10^6 \text{ Hz/sec}$$

CARRIER LOOP BANDWIDTH
VS
INPUT SIGNAL POWER
AND
RANGE



-10A-

27 April 1971

The maximum time (T_L) to lock for the Interrogator is calculated

$$T_L = \frac{2(34 \text{ kHz})}{1270 \text{ kHz/sec}} = 53 \text{ milliseconds}$$
$$\text{Avg } T_L = 27 \text{ Ms.}$$

The maximum time (T_L) to lock for the Transponder is

$$T_L = \frac{2(29 \text{ kHz})}{1270 \text{ kHz/sec}} = 45 \text{ milliseconds}$$
$$\text{Avg. } T_L = 23 \text{ Ms.}$$

3.2.4 Range-Rate (R) Data Servo Loop

3.2.4.1 Dynamics

The maximum doppler and doppler rate as seen by the range-rate servo input is the carrier rate divided by 128

$$d_{\text{max.}} = \frac{\pm 113 \text{ kHz}}{128} = \pm 880 \text{ Hz}$$

$$a_{\text{max.}} = \frac{\pm 4.5 \text{ kHz/sec}}{128} = \pm 35 \text{ Hz/sec.}$$

3.2.4.2 R Servo Loop Bandwidth

The bandwidth of the CIRIS Range Rate Servo is $B_L = 200 \text{ Hz}$. This bandwidth would handle the acceleration requirements and SNR requirements but the high doppler rates would require over 1/2 second to pull into lock. Simply widening the loop bandwidth to $B_L = 500 \text{ Hz}$ would improve lock time and settling time, and would not degrade the measurable SNR (See Paragraph 3.2.4.4).

27 April 1971

The approximate pull in time for this servo is

$$T_P \approx \frac{(\Delta\omega)^2}{2\zeta \omega_n^3} \approx \frac{4.2 (\Delta f)^2}{B_L^3} \text{ sec}$$

$$T_P \approx \frac{4.2 (880)^2}{(500)^3} \approx 25 \text{ milliseconds}$$

The lockup transient occupies a time on the order of $1/\omega_n$ seconds = 1 milliseconds

The maximum measurable loop settling time (t) is derived using the loop resolution of 1/2048

$$1/2048 \approx \exp(-t\omega_n/2\zeta)$$

$$t \approx (0.015) (7.6) \text{ seconds} \approx 11 \text{ milliseconds}$$

Total time allotted = 37 milliseconds maximum

For all tracking other than orbital this time is 12 milliseconds maximum.

3.2.4.3 Range Rate SNR

The signal-to-noise ratio in the carrier loop is +10 dB at a noise bandwidth of 1 kHz. Since the input to the data servo comes from the VCL0 in the carrier receiver, the signal input to the servo is 128 times better, i.e., 10 dB + 42 dB = +52 dB in a 1 kHz noise bandwidth. No improvement is provided by the 1000-Hz noise bandwidth of the range rate servo. Therefore, the range rate servo loop SNR is +52 dB.

The required SNR in the range rate servo for $1\sigma = 0.03$ ft/sec error over a one second count period is calculated by

$$\text{SNR} = 1/2\sigma^2$$

27 April 1971

$$\sigma = .03 \frac{\text{Ft}}{\text{sec}} \times \frac{1}{\text{Resolution}} \frac{\text{Ft}}{\text{Bits}} \times \frac{\text{Radians}}{\text{Bit}}$$

$$\text{where Resolution} = \frac{C}{2(16) f_T} = \frac{9.8 \times 10^8}{2(16) 2.2 \times 10^9} \approx 0.14 \text{ Ft/Bit}$$

Therefore,

$$\sigma = (.03) \frac{\text{Ft}}{\text{Sec}} \times \frac{1}{0.14 \text{ Ft/Bit}} \times \frac{2\pi \text{ radians}}{2048 \text{ Bits}} = 0.0657 \text{ rad.}$$

Therefore

$$\text{SNR} = \frac{1}{2\sigma^2} = \frac{1}{2(0.0657)^2} = 11600 = 41 \text{ dB}$$

3.2.4 External Noise Error

The actual phase jitter due to external noise at threshold (+52 dB) is

$$\sigma = \frac{1}{\sqrt{2 \text{ SNR}}} = \frac{1}{\sqrt{2(15.7) 10^4}} = 0.0178 \text{ radians}$$

Converting this phase error to feet over a 1-second count period gives

$$1\sigma = 0.0178 \text{ rad/sec} \times \frac{0.3 \text{ ft.}}{0.0657 \text{ rad}} = .008 \text{ ft/sec}$$

3.2.5 Range Rate Counter

The range rate counter will be increased by 2 stages to 22 stages
 $2^{22} = 4,194,304$

$$\text{Bit Storage} = \frac{2(25,000 \text{ ft/sec})}{0.14 \text{ ft/Bit}} = 3.6 \times 10^6 \text{ Bits}$$

3.2.6 Range Data Servo Loop

3.2.6.1 Dynamics - The maximum doppler and doppler rates as seen by the range servo input is

$$d_{\text{max}} = \pm 2 \frac{v}{c} f = 12.3 \text{ Hz}$$

27 April 1971

where,

v = maximum velocity (25,000 ft/sec)

c = velocity of propagation (9.8×10^8 ft/sec)

f = fine modulating frequency (240 kHz)

$$a_{\max} = \pm 2 \frac{vt_{\max}}{c} f = 0.49 \text{ Hz/sec}$$

where,

$$v/c_{\max} = 1,000 \text{ ft/sec}^2$$

3 2 6.2 Required Loop Bandwidth

The loop bandwidth is chosen to keep the peak error less than 0.5 feet at maximum acceleration, or

$$\theta_a = 0.5 \text{ ft} \times \frac{2\pi}{2048} = 0.00154 \text{ radians (maximum)}$$

The loop natural frequency ω_n is calculated from

$$\omega_n^2 = \frac{\Delta \dot{\omega}}{\theta_a} = \frac{0.49 (2\pi)}{0.00154}$$

$$\omega_n = 45 \text{ radians}$$

Setting the damping factor ζ to 0.707,

$$B_L = \frac{\omega_n}{2} \zeta + \frac{1}{4\zeta} \text{ Hz} = 25 \text{ Hz minimum}$$

Examining the settling time for this loop bandwidth

$$1/2048 = \exp(-t/2 \zeta/\omega_n)$$

$$t = 7.6 (0.0295) = 0.238 \text{ sec}$$

27 April 1971

3 2.6 3 SNR and External Noise Error

From an operational view it would be better to reduce the settling time by opening the bandwidth of the servo if sufficient signal-to-noise exists so as not to degrade the measurable accuracy or cause ambiguous range measurements. The data output SNR in the receiver is improved by the square of the index β . For the fine tone $\beta = 20$ and $\beta^2 = 26$ dB. For the four coarser tones, $\beta = 2$ and $\beta^2 = 6$ dB. Thus

$$\text{SNR (fine tone)} = 10 \text{ dB} + 26 \text{ dB} = 36 \text{ dB} + \text{Bw improvement}$$

$$\text{SNR (other 4 tones)} = 10 \text{ dB} + 6 \text{ dB} = 16 \text{ dB each} + \text{Bw improvement}$$

The SNR of the fine tone is treated separately for bandwidth improvement thus

$$\text{Bw improvement} = \frac{500 \text{ Hz}}{25 \text{ Hz}} = 20 = 13 \text{ dB}$$

Thus at threshold

$$\text{SNR (fine tone)} = 36 + 13 = 49 \text{ dB} = 8 \times 10^4$$

The phase jitter is

$$1\sigma = \frac{1}{\sqrt{2 \text{ S/N}}} = \frac{1}{\sqrt{2 (8) 10^4}} = 0.025 \text{ radians}$$

Converting to feet of jitter

$$1\sigma = 0.025 \text{ radians} \times \frac{2048 \text{ ft}}{2\pi \text{ rad}} = 82 \text{ ft}$$

The bandwidth of the coarser tones is a compromise considering the 3-Sigma or peak-to-peak jitter, settling time and accuracy of time of reading in sequential mode at maximum velocity. The bandwidth of about 50 Hz is a good compromise and is only 10 Hz wider than the CIRIS 40 Hz servos.

27 April 1971

$$\text{The Bw improvement} = \frac{500 \text{ Hz}}{50 \text{ Hz}} = 10 = 10 \text{ dB}$$

Thus at threshold

$$\begin{aligned} \text{SNR (Coarser Tones)} &= 16 \text{ dB} + 10 \text{ dB} = \\ 26 \text{ dB} &= 4 \times 10^2 \end{aligned}$$

The phase jitter is

$$1\sigma = \frac{1}{\sqrt{2 \text{ S/N}}} = \frac{1}{\sqrt{2 (4) 10^2}} = .0354 \text{ radians}$$

Converting to bits of jitter

$$1\sigma \text{ Bits} = .0354 \text{ radians} \times \frac{2048 \text{ Bits}}{2\pi \text{ rad}} = 12 \text{ Bits}$$

This corresponds to a peak-to-peak jitter of 36 bits and since the ambiguity resolution algorithm corrects up to ± 128 bits ample safety margin or 85% of the maximum timing error in sequential sampling can be allotted to the actual measurement of the particular coarser tone. The maximum error in time of sampling of the coarser tones is

$$T_{\text{max}} = 1/2 \frac{\text{Range (fine tone)}}{\text{Max. Velocity}} = \frac{1/2 \cdot 2048 \text{ ft}}{25,000 \text{ ft/sec}} =$$

41 milliseconds

Maximum time error of sampling 85 (41) \approx 35 milliseconds

3 2 6 4 Lock-up Transient and Settling Time

Fine Tone

The lock transient is $1/\omega_n = 1/45 = 22$ milliseconds

Settling time is from paragraph 3 2.5 2 equal to 238 milliseconds

Total Delay = 238 + 22 = 260 Milliseconds

27 April 1971

Coarser Tones

The lock transient is $1/94 \approx 11$ Milliseconds

Settling time

$$1/2048 = \exp(-t\omega_n/2\zeta)$$

$$t = 7.6 (.0151) = 115 \text{ Milliseconds}$$

Total Delay Each Tone = 126 Milliseconds

3.2.6.5 Velocity Error

The velocity coefficient K_v is.

$$K_v = K_o K_d F(o) = 130 \text{ dB} = 3 \times 10^6$$

where K_o = VCO sensitivity = 63 rad/sec/volt

K_d = phase detector sensitivity = 5 volt/rad

$F(o)$ = gain of operational amplifier = 100 dB

The phase error due to velocity is

$$\theta_v = \frac{\Delta \omega}{K_v}$$

The sum of all the drifts ($\Delta \omega$) is

$$\text{doppler (max)} = \pm 12.3 \text{ Hz} \times 2\pi = 78 \text{ rad/sec}$$

$$\text{VCO } (5 \times 10^3 \text{ ppm}) = \pm 20 \text{ Hz} \times 2\pi = \underline{126 \text{ rad/sec}}$$

$$\text{Total } \Delta \omega = 204 \text{ rad/sec}$$

$$\text{then } \theta_v = \frac{204}{3 \times 10^6} = 68 \times 10^{-6} \text{ radians}$$

$$\text{and } \theta_v = \frac{68 \times 10^{-6}}{3 \times 10^{-3}} \approx 0.02 \text{ ft}$$

3.2.7 System Acquisition

3.2.7.1 Data Link

The CIRIS data link can be easily modified to the space shuttle requirements. The bandwidth is decreased to improve bit error rate at the expense of some acquisition time. The maximum number of transponders with the standard 8-bit code length is decreased by a factor of 4 to 63 transponders as two bits are allocated to the high/low power mode and slow/fast sweep mode. Also one of the available 64 codes is reserved for internal calibration as in CIRIS. It should be pointed out here that a maximum of 63 transponders was considered adequate for mission purposes. The code length could be expanded to handle any number of transponders.

A bit rate of 1 kilobits per second is chosen as a compromise between required transmission time and SNR. A subcarrier is frequency modulated at an index of 1 in accordance with the bit code, bit timing and message synchronizing. The subcarrier is phase modulated on the carrier. The same message organization and data rate used in CIRIS is proposed here for simplification in hardware and lower cost.

3.2.7.2 Data Link SNR

When the data link subcarrier is on (acquisition), the range data feedback loop is open, thereby eliminating data loop noise contribution. The carrier-to-noise in the rf. at an index of 1 is -20 dB (See Table 3.2) in a noise bandwidth of 1.5 MHz. The data link SNR then is

$$S/N_0 = c/N_1 \frac{B_L (if)}{B_L (DL)} \beta^2 = +12 \text{ dB}$$

where

$$c/N_1 = \text{carrier-to-noise in if.} = -20 \text{ dB}$$

$$B \text{ (if)} = \text{if. bandwidth} = 1.5 \text{ MHz}$$

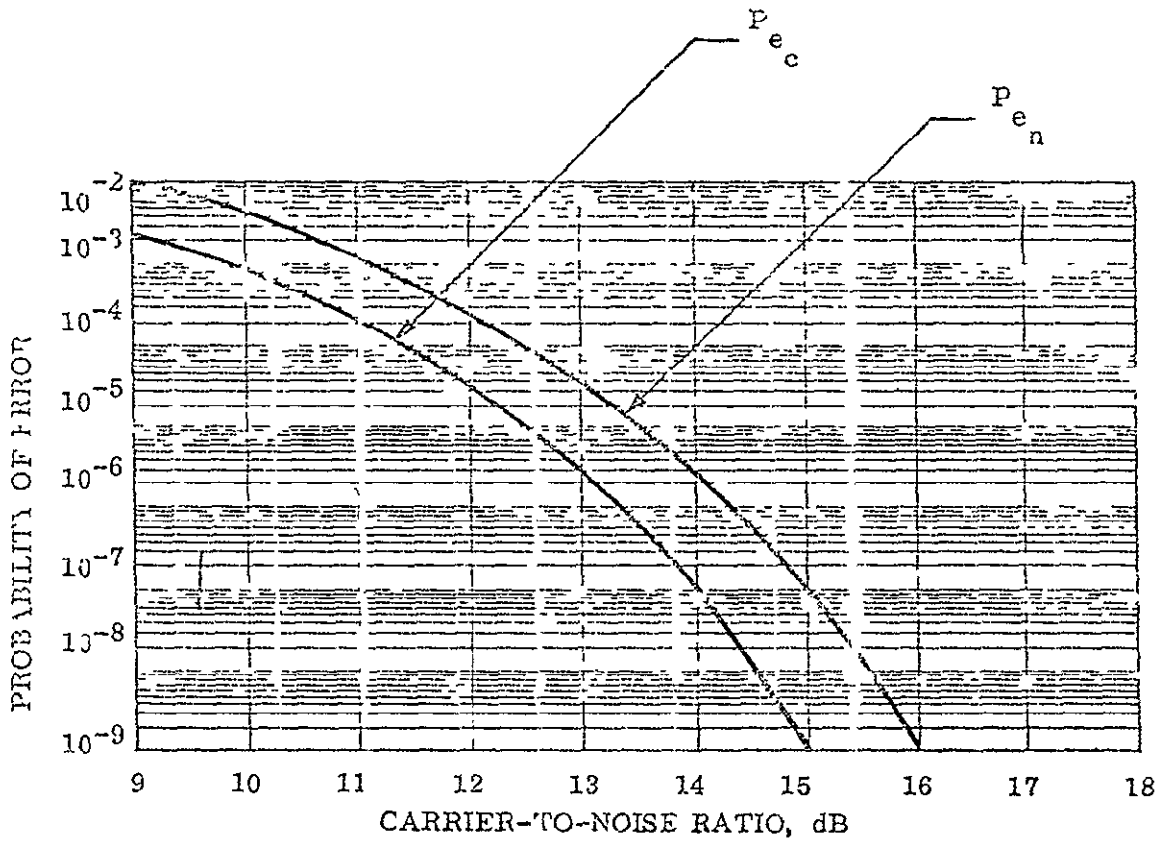
$$B_L \text{ (DL)} = \text{data link bandwidth} = 1.0 \text{ KHz}$$

3.2.7.3 Probability of Error

The derivation of the expressions for the probability of error in frequency shift key (FSK) systems is quite involved and will not be given here. Figure 2-1 plots the carrier-to-noise ratio (dB) versus probability of error. (ref Philip F. Panter, Modulation, Noise, and Spectral Analysis, McGraw-Hill, 1965, p. 714.) This curve shows that an S/N of 12.5 dB in a coherent FSK system provides a probability of error of 10^{-5} .

3.2.7.4 Code Acquisition Time

The message code (transponder ID, $\overline{hi/lo}$ power and slow/fast sweep) is 8 bits plus sync for a total of 9 bits. Since two sync bits must be received for a transponder response the minimum time for code acquisition is $10 \text{ bits}/250 \text{ bits/sec} = 40 \text{ ms}$. The maximum time is $18/250 = 72 \text{ ms}$. Average time $(72 + 40)/2 = 56 \text{ ms}$.



Legend:

P_{e_n} = probability of error for noncoherent FSK system.

P_{e_c} = probability of error for a coherent FSK system.

Figure 2-1. Probability of Error in Binary FSK Systems

3.2.8 Calibration

The RRS determines range based on measurements of signal phase change. It is necessary, therefore, to remove the fixed phase delays attributable to the interrogator (ϕ_I), to the transponder (ϕ_T), and to the antennas and their cables from the total measurable phase delay before determining range from the range phase delay (ϕ_R). These fixed equipment phase delays are measured by use of two calibration procedures - an internal calibration, and a loop calibration. Figure 2-2 provides a functional representation of the phase delays involved.

3.2.8.1 Calibration Modes

The internal calibrate mode measures ϕ_I by phase-locking the interrogator receiver to its own transmitter. In this mode, a signal of the proper frequency is coupled to the interrogator receiver through the antenna circulator. The calibration signal then is processed in the same manner as a ranging signal.

The loop calibration mode measures range between the interrogator and transponder when they are separated by a path of known range. This procedure measures the total combination of phase delays

$$\phi_{\text{measured}} = \phi_R + \phi_I + \phi_A + \phi_T$$

Subtracting the known ϕ_R and the ϕ_I as measured during internal calibrate results in

$$\begin{aligned} \phi_{\text{measured}} - \phi_R (\text{known}) - \phi_I (\text{int cal}) = \\ \phi_A + \phi_T \end{aligned}$$

27 April 1971

The transponder is a completely closed-loop, phase-locked device and, as such, its phase delay (ϕ_T) remains stable or constant. Similarly, ϕ_A remains constant as long as the antennas and their cables remain the same electrical length. The combination $\phi_A + \phi_T$ then represents the fixed part of the calibration constant.

The interrogator calibration contribution ϕ_I on the other hand, may drift slowly with time due to temperature changes or component aging. This drift occurs primarily in the interrogator circuits, which are not part of the receiver's feedback loop.

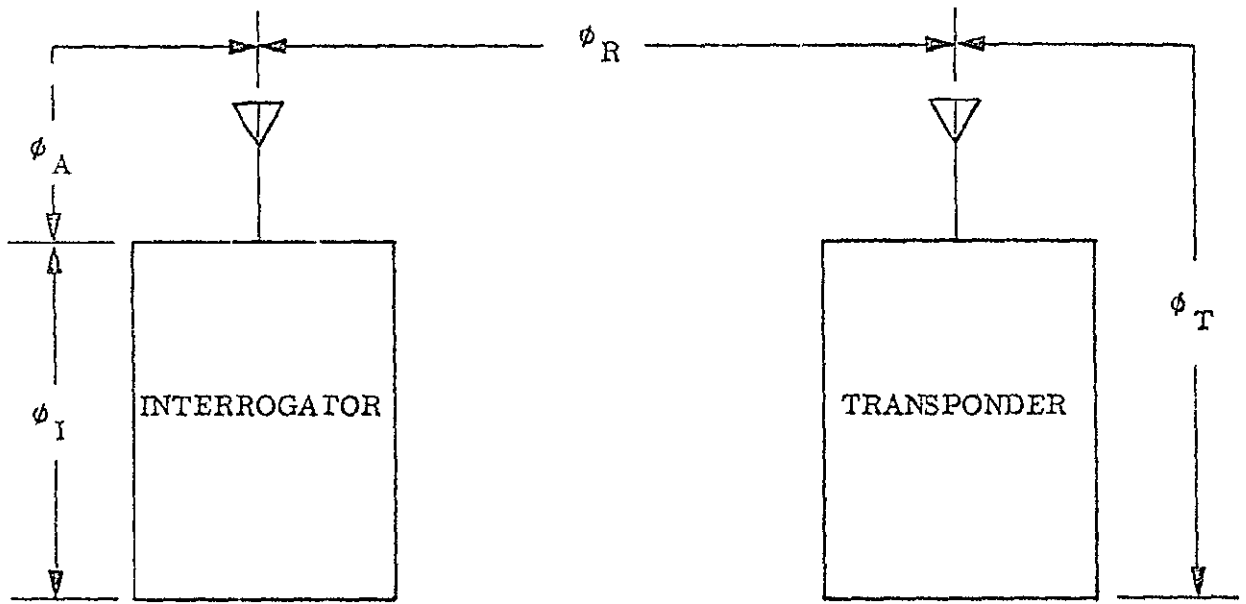
During system operation, interrogator drift is compensated by performing internal calibrations to measure ϕ_I . These values of ϕ_I are compared with the value recorded during loop calibration, and if any change has occurred the calibration word is adjusted accordingly.

To summarize, the calibration word is made up of two parts: (a) a constant portion due to phase delay in the transponder, antennas, and cables, and (b) a drift-prone portion due to the interrogator. The constant portion is determined once only, during internal loop calibration. The drift-prone portion is monitored and adjusted frequently by internal calibration.

$$[\text{CAL WORD}] = [\phi_A + \phi_T]_{\text{loop cal}} + [\phi_I]_{\text{int cal}}$$

In the operate mode, range phase delay is computed by subtracting the calibration word from the total phase delay measured by the RRS, thus,

$$\phi_R = \phi_{\text{measured}} - [\text{CAL WORD}]$$



Where

$$\phi_{\text{measured}} = \phi_I + \phi_A + \phi_R + \phi_T$$

ϕ_{measured} = total measured phase delay

$$\phi_R = \phi_{\text{measured}} - [\phi_I + (\phi_A + \phi_T)]$$

ϕ_I = Interrogator internal delay

True	Measured	Calibration	$(\phi_A + \phi_T)$ = Constant delay of antennas and transponder
Range	Delay	Figure	

Figure 2-2. Calibration Setup for Radio Reference Subsystem

3 2 8 2 Calibration Accuracy

If calibration is attempted using a known air link path between interrogator and transponder, the calibration accuracy will be dependent on the air link path ϕ_R during such loop calibration. Since multipath then becomes a great source of error, the system is more accurately calibrated with a cable link of known electrical length. This type calibration need be conducted only once to determine the constant $\phi_A + \phi_T$. It is then set into the computer as a known constant.

This type of loop calibration is a factory or depot-level task, and should not normally be attempted at the field maintenance level. On the other hand, internal calibration can and should be performed several times during system operation in order to compensate for any drift in the interrogator.

Using the cabling method, the transponder and cables can be calibrated to a maximum error of one foot. The interrogator can also be calibrated to this same accuracy of one foot.

3 2 9 Drift Considerations

3 2 9 1 Transponder

The transponder is a completely closed-loop phase-locked device with range modulation feedback of 30 dB. Any drifts would be reduced by that amount. Extensive tests have shown that the transponder drifts are less than the readout capability of one foot.

3 2 9 2 Interrogator

Drifts in the interrogator are removed by the internal calibration scheme. The drifts occur slowly with time due to temperature changes or component aging. With internal calibration performed several times during mission a maximum drift value of one foot will be assigned to the error budget.

3 2 10 Oscillator Stability

The stable reference oscillation for both the carrier and range modulation are temperature-compensated crystal oscillators requiring no warm-up time or over power. Frequency stability versus temperature (-40° to +70°C) is 1 ppm. Stability versus time is 1 pp 10⁸ per day, 1 ppm per year.

3 2 10 1 Contribution to Range Error

At 1 pp 10⁷ oscillator error, the range error at the maximum range of 1500 nautical miles is 1 foot. With long-term stability of 1 ppm per year, the system could be unattended for one year before the oscillator would drift beyond 1 ppm.

3 2 10 2 Contribution to Range Rate Error

At 1 ppm oscillator error, the maximum rate error occurs at maximum velocity or 25,000 ft/sec X 10⁻⁶ = 0.025 ft/sec. Thus, stability requirements on carrier oscillator is not as stringent.

3 2 11 Equipment Noise

The phase error due to equipment noise would be difficult and probably inaccurate to calculate. Laboratory measurements were taken to detect the presence of noise. For testing purposes,

the equipment was operated with a signal input at high signal-to-noise ratio (≈ -60 dBm input signal). Any remaining measured jitter was defined as equipment noise. The jitter was observed on an oscilloscope by monitoring the least significant flip-flop of the fine range servo and synchronizing the oscilloscope to the reference. The peak-to-peak time jitter was observed at less than 60 nanoseconds corresponding to approximately 0.5 ft p-p jitter at a VCO frequency of 7.7 MHz.

The corresponding flip-flop in the range rate servo indicated a p-p time jitter of less than 50 nanoseconds corresponding to less than 0.01 ft/sec at a VCO frequency of 10 MHz.

3.2.12 Multipath Error

A source of range error in any CW precision tracking system arises when the signal is received from more than one propagation path by reflection from the ground or nearby objects. This phenomenon known as multipath reception can cause phase errors in a DME and possible ambiguous range measurement if the phase error is larger than the phase overlap of the modulation frequencies. Many authors have discussed the effects of multipath on FM signals. (A detailed discussion of these effects is contained in Appendix A.)

Multipath is a function of geometry, the reflection coefficient of the earth's surface, and the roughness of the reflection point. The range error or amount of phase shift caused by this multipath is dependent on the modulation index along with the vector addition of the multipath.

It is significant to note that from figures 4, 6 and 7 of Appendix A that the maximum phase error is $\approx 5^\circ$ at an index of 20 with the reflection coefficient a maximum of 1. This corresponds to a maximum error of

$$5^\circ \times 5.7 \text{ ft/deg} = 28.5 \text{ ft}$$

This absolute maximum value of α is misleading and does not indicate typical values. Typical values of α were measured experimentally as $R = 0.1$ by SHIRAN (AN/USQ-28) tests. From Figure 7 of Appendix A this would cause a phase error of about 0.35° corresponding to a distance error of

$$0.35^\circ \times 5.7 \text{ ft/deg} = 2 \text{ ft}$$

Ground testing of the CR-100 subsystem indicates and supports this number for ground-to-ground measurements.

The maximum error that could ever be observed in range-rate measurements due to multipath would be a change in multipath during the 1-second count period that would cause the phase error on the carrier to change by 90° . * This would cause an error maximum of

$$90^\circ \times \frac{0.02 \text{ ft/sec}}{22.5^\circ} = 0.08 \text{ ft/sec}$$

Carrier multipath normally appears as a slow fading or null in carrier signal strength. The phase error rate of the carrier is therefore quite slow. Not enough data exists to assign an absolute value on this error. If one can assume a reflection coefficient change of 0.1 as typical then an error of 0.01 ft/sec would be a reasonable number.

3.2.13 Atmospheric Refractive Index

The refractive index determines the propagation of electromagnetic waves and also determines the wavelength of electromagnetic waves of a given frequency. In order to correctly convert phase measurement into range one must know the refractive index. Any error in the refractive index results in a corresponding scale factor error in the range measurement.

The if atmospheric refractive index varies with pressure, temperature, and water vapor content. The accuracy that one can determine these variables will of course affect the ultimate accuracy.

* A larger error would break carrier lock and cause the data quality indicator to flag the sample as bad data.

Appendix B Tropospheric and Ionospheric Propagation Effects on Range Measurement is a detailed analysis of the propagation effects on slant-range measurements produced by range measuring equipment operating in the 1.5 - 2.25 GHz frequency range

Appendix C Tropospheric Propagation Effects on Range Rate Measurements is a detailed analysis of two study cases

3.2.14 Range Reference Zero-Crossing Error

The range data is read on the zero crossing of the range reference counter. Since this actual time of reading range is delayed beyond the read signal (R-STOP) by a maximum time t_{\max} of

$$t_{\max} = \frac{1}{f} = \frac{1}{3.751 \text{ kHz}} = 267 \text{ microseconds}$$

Assuming a maximum aircraft velocity of 2000 ft/sec directly toward or away from the transponder, the maximum error in range, ΔR_{\max} is

$$\Delta R_{\max} = 2000 \text{ ft/sec} \times 267 \times 10^{-6} \text{ sec}$$

Assuming the worst case in aircraft vector dynamics and a maximum of 267 μ s in determining the time of reading of range, yields

$$\sigma = 0.2 \text{ ft (max } v)$$

The error at maximum orbital velocity is

$$\Delta R_{\max} = 25000 \text{ ft/sec} \times 267 \times 10^{-6} \text{ sec} = 6.7 \text{ feet}$$

Producing an uncertainty of $1\sigma = 0.2$ feet. If required, this could be eliminated by several minor hardware changes: i.e. reading reference and data immediately on command counting time between R-Stop command and Range read or providing a range lead command output

APPENDIX A
EFFECTS OF MULTIPATH IN DISTANCE
MEASUREMENT SYSTEMS

A source of noise in any CW precision tracking system arises when the signal is received from more than one propagation path by reflection from either the ground or nearby objects. This phenomenon known as multipath reception can cause phase errors in a DME and possible ambiguous range measurement if the phase error is larger than the phase overlap of the modulation frequencies. Many authors have discussed the effects of multipath on FM signals.

The documentation on this subject is sufficiently clear. Therefore, only a summary is presented. In particular, the work of Sollenberger will be followed and some of the numerical results are reproduced here. An FM signal can be represented by:

$$E = E_0 \exp j \left[\int_0^t \omega dt \right]$$

$$\omega = \omega_c + \Delta \omega \cos \omega_m t$$

where ω_c is the carrier angular frequency, ω_m is the modulation angular frequency, and $\Delta \omega$ is the frequency deviation of the carrier due to the modulation.

When two signals are present, one due to a direct wave, the other from a reflected wave, the total signal is

$$E_c = E_d + E_r$$

$$E_c = E_0 \exp j \left[\int_0^t \omega dt \right] + RE_0 \exp j \left[\int_0^{t+t_d} \omega dt + \phi \right]$$

Assuming that the path attenuation due to the different path lengths is not significantly different, t_d is the time delay of the reflected signal and $R \angle \phi$ is the complex coefficient of reflection. The instantaneous phase of the composite signal can be most easily determined from figure 1. Letting:

$$b_1 = \int_0^t \omega dt$$

$$b_2 = \int_0^{t+t_d} \omega dt + \phi, \text{ and}$$

$$b = b_1 + \tan^{-1} \left[\frac{R \sin (b_2 - b_1)}{1 + R \cos (b_2 - b_1)} \right]$$

The receiver output is proportional to:

$$e_d \approx \omega_c - \frac{db}{dt}$$

$$\approx \Delta \omega \cos \omega_m t + \frac{d}{dt} \tan^{-1} \left[\frac{R \sin (b_2 - b_1)}{1 + R \cos (b_2 - b_1)} \right]$$

The first term contains the desired information and the second term is a distortion term arising from the multipath. By expanding the arctan term into a series using the proper trigonometric identities and letting:

$$B = \omega_m \left[t + \frac{t_d}{2} \right]$$

$$Z = 2\beta \sin \left[\frac{\omega_m t_d}{2} \right]$$

$$\beta = \frac{\Delta f}{f_m}$$

$$\theta_o = -\omega_c t_d + \varphi$$

then

$$\frac{d}{dt} \tan^{-1} \left[\frac{R \sin (b_2 - b_1)}{1 + R \cos (b_2 - b_1)} \right]$$

becomes

$$\omega_m \sum_{m=1}^{\infty} S_m \sin 2mB + \omega_m \sum_{m=0}^{\infty} C_m \sin (2m+1)B$$

$$S_m(\theta_o, R, Z) = (-1)^m 4m \sum_{n=1}^{\infty} \frac{(-R)^n}{n} \sin n\theta_o J_{2m}(nZ)$$

$$C_m(\theta_o, R, Z) = -(-1)^m 2(2m+1) \sum_{n=1}^{\infty} \frac{(-R)^n}{n} \cos n\theta_o J_{2m+1}(nZ)$$

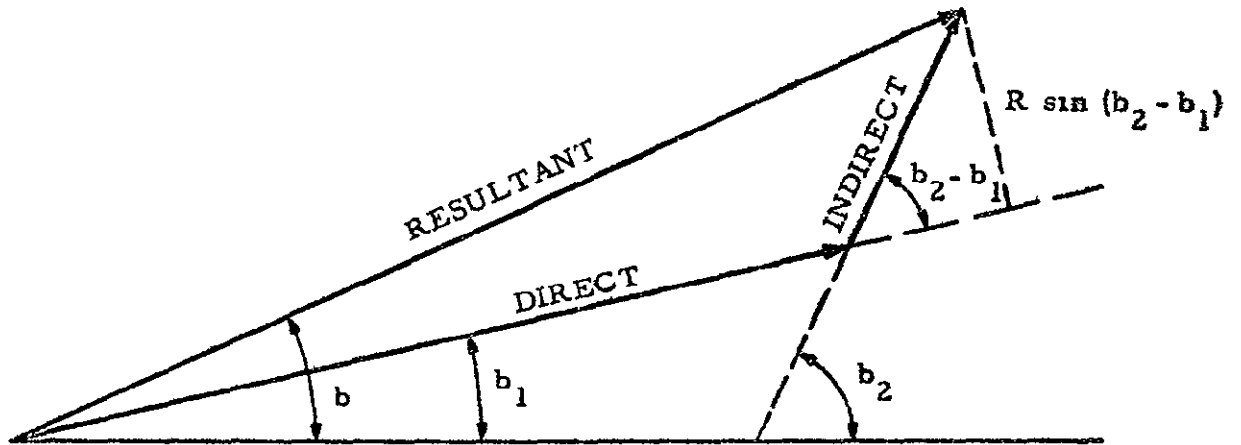


Figure 1 Addition of Direct and Indirect FM Wave

This includes the harmonic components at both the carrier and modulation frequencies. The harmonics of the carrier are filtered out in the receiver before reaching the phase discriminator. Then, using only the fundamental (carrier, $m = 0$) and manipulating the form of the output signal equation so that it represents the desired signal plus a phase term due to multipath, the following expression can be derived.

$$e_d \approx \Delta \omega A \cos \left[\omega_m t - \alpha \right]$$

where

$$\alpha = \tan^{-1} \left[\frac{\frac{C_o}{\beta} \cos \frac{\omega_m t_d}{2}}{1 - \frac{C_o}{\beta} \sin \frac{\omega_m t_d}{2}} \right]$$

$$C_o(\theta_o, R, Z) = -2 \sum_{n=1}^{\infty} \frac{(-R)^n}{n} \cos n\theta_o J_1(nZ)$$

In this expression, θ_o and Z , defined previously, represent components at the carrier and the modulation frequencies respectively. A is a

complex amplitude fluctuation but is made constant by limiting in the receiver α is the phase error due to multipath that will be measured by the phase discriminator. The details of the derivation for α are complex but can easily be followed.

The expression for α is a complex function of B and R involving a series of Bessel functions and sine terms that have oscillations at both the carrier and the modulation frequencies. A complete numerical solution of this equation would involve a complex computational program. Instead it is possible to estimate maximum excursions of α based on values of C_o , R, B, and t_d . This has been done in a very useful fashion and the portions of the study of interest to SHIRAN will be repeated here. The quantity $\frac{X}{\omega_c}$ is substituted for t_d in the equations below with the results

$$\alpha = \tan^{-1} \left[\frac{\frac{C_o}{\beta} \cos \frac{X \omega_m}{2 \omega_c}}{1 - \frac{C_o}{\beta} \sin \frac{X \omega_m}{2 \omega_c}} \right]$$

$$C_o(X, R, Z) = -2 \sum_{n=1}^{\infty} \frac{(-R)^n}{n} \cos n(X - \phi) J_1(nZ), \text{ and}$$

$$Z = 2\beta \sin \left(\frac{\omega_m X}{\omega_c 2} \right)$$

Inspection of the equation for α reveals that oscillations at the carrier frequency (related to X) can be expected and the oscillations at the modulation frequency (contained in Z) will form an envelope for the faster oscillation at the carrier frequency.

For $\frac{\omega_m}{\omega_c}$ very small (which will be the case for any possible combination of frequencies for the DME) it can be seen that $J_1 \left(2n\beta \sin \frac{\omega_m X}{\omega_c 2} \right)$ is nearly constant over increments of X of the order of 0 to 2π . Then $C_o(X, R, Z)$ can be determined for small values of X by letting Z be constant. The result is given in figure 2 which illustrates the fast oscillations. C_o has maxima and minima

NOTE. TAKEN FROM "GROUND-REFLECTION PHASE ERRORS OF CW-FM TRACKING SYSTEMS" BY T. E. SOLLENBERGER

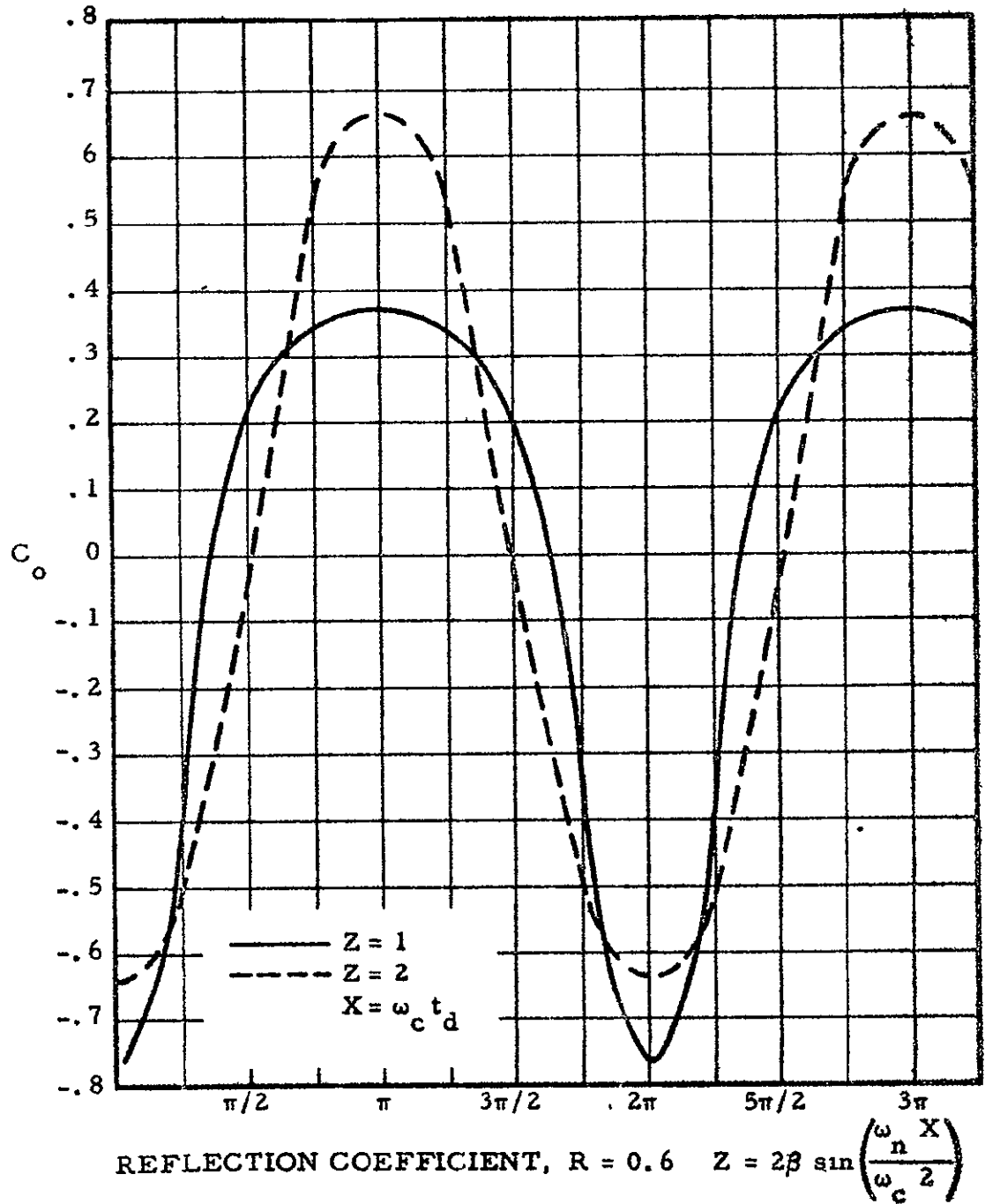


Figure 2 Function $C_o = -2 \sum_{n=1}^{\infty} \frac{(-R)^n}{n} \cos nX J_1(nZ)$ with Z Constant

when X equals integral multiples of π . Thus, if $X=0$ or π , $C_o(X, R, Z)$ can be computed for various Z, and maximum values of C_o can be found which will represent the peaks of the envelope or the slow oscillations. Figure 3 contains C_o as a function of Z for various R, ignoring the fast oscillations of figure 2 by using only the values of $C_o(\pi, R, Z)$ and $C_o(0, R, Z)$.

It can be seen that C_o can never exceed 2 for any X or Z. Then,

$$\alpha_{\max} = \tan^{-1} \left[\frac{\frac{C_o}{\beta} \cos \frac{\omega_m X}{\omega_c Z}}{1 - \frac{C_o}{\beta} \sin \frac{\omega_m X}{\omega_c Z}} \right]$$

and α is maximized when $\sin \frac{\omega_m X}{\omega_c Z} = \frac{C_o}{\beta}$.

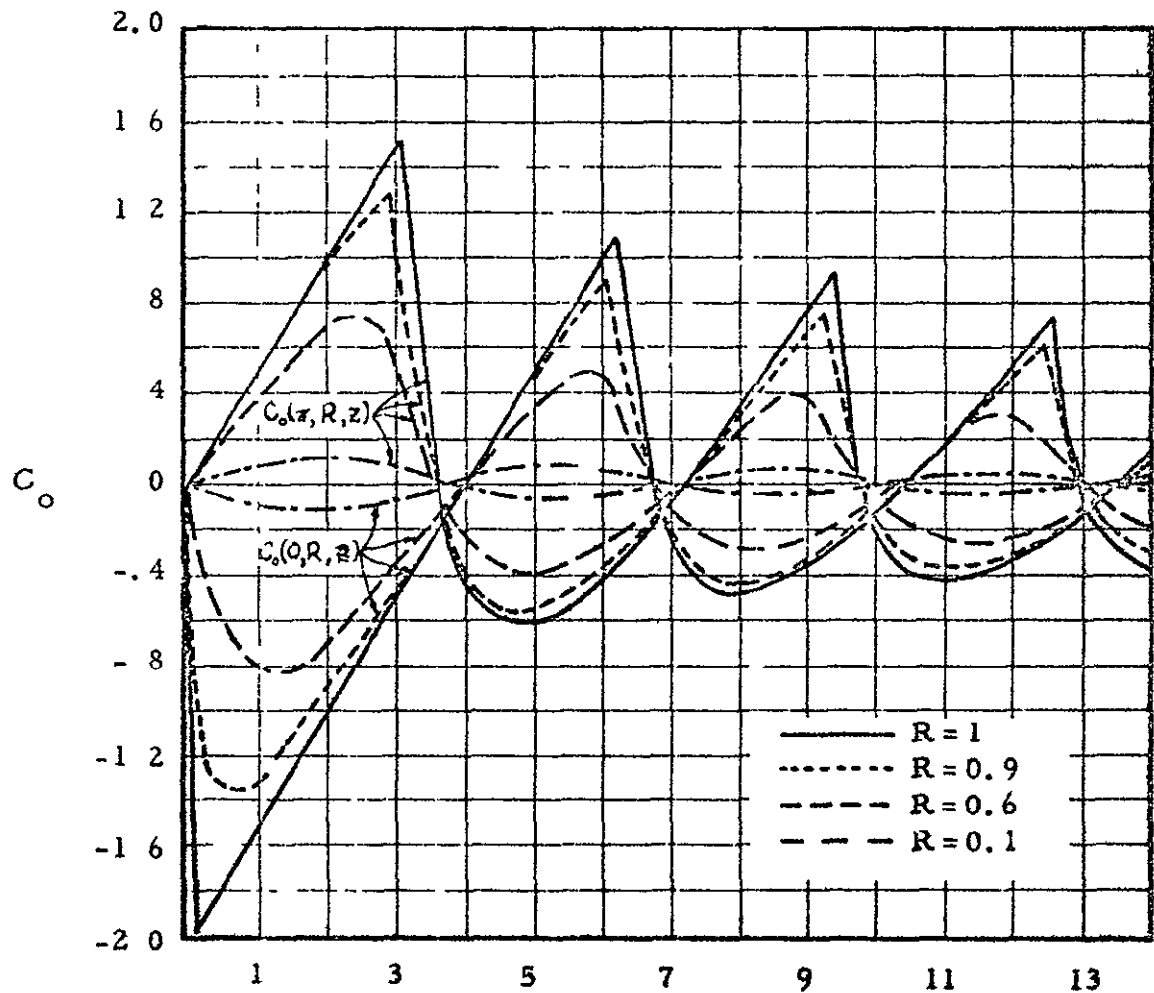
Thus:
$$\alpha_{\max} = \tan^{-1} \left[\frac{\frac{C_o}{\beta}}{1 - \left(\frac{C_o}{\beta}\right)^2} \right] \text{ for } C_o \text{ constant.}$$

This expression will yield the maximum value that α can achieve for a given modulation index and reflection coefficient. Figure 4 shows this relation as a function of the modulation index and was obtained by using the maximum value of C_o for values of R = 1.0, 0.9, and 0.6. (The value of R = 0.1 shown on figure 4 was measured experimentally)

Figure 4 gives only the absolute maximum value of α and does not indicate typical values of α at combinations of path delay, modulation frequency, reflection coefficient, etc., at other than the worst conditions.

To plot α as a function of X, or Z, first consider Z constant for small changes in X as was done previously for the determination of C_o . It can then be seen that α has periodic maximums and minimums at integral multiples of X as did C_o . Ignoring the fast oscillations of α with X, figure 5 shows a half cycle of the slow

NOTE TAKEN FROM "GROUND-REFLECTION PHASE ERRORS OF CW-FM TRACKING SYSTEMS" BY T E SOLLENBERGER,



R = REFLECTION COEFFICIENT

$$Z = 2\beta \sin\left(\frac{\omega_m X}{\omega_c 2}\right)$$

Figure 3 The Functions, $C_o(\pi, R, Z) = -2 \sum_{n=1}^{\infty} \frac{(-R)^n}{n} J_1(nZ)$ and

$$C_o(0, R, Z) = -2 \sum_{n=1}^{\infty} \frac{(-R)^n}{n} J_1(nZ).$$

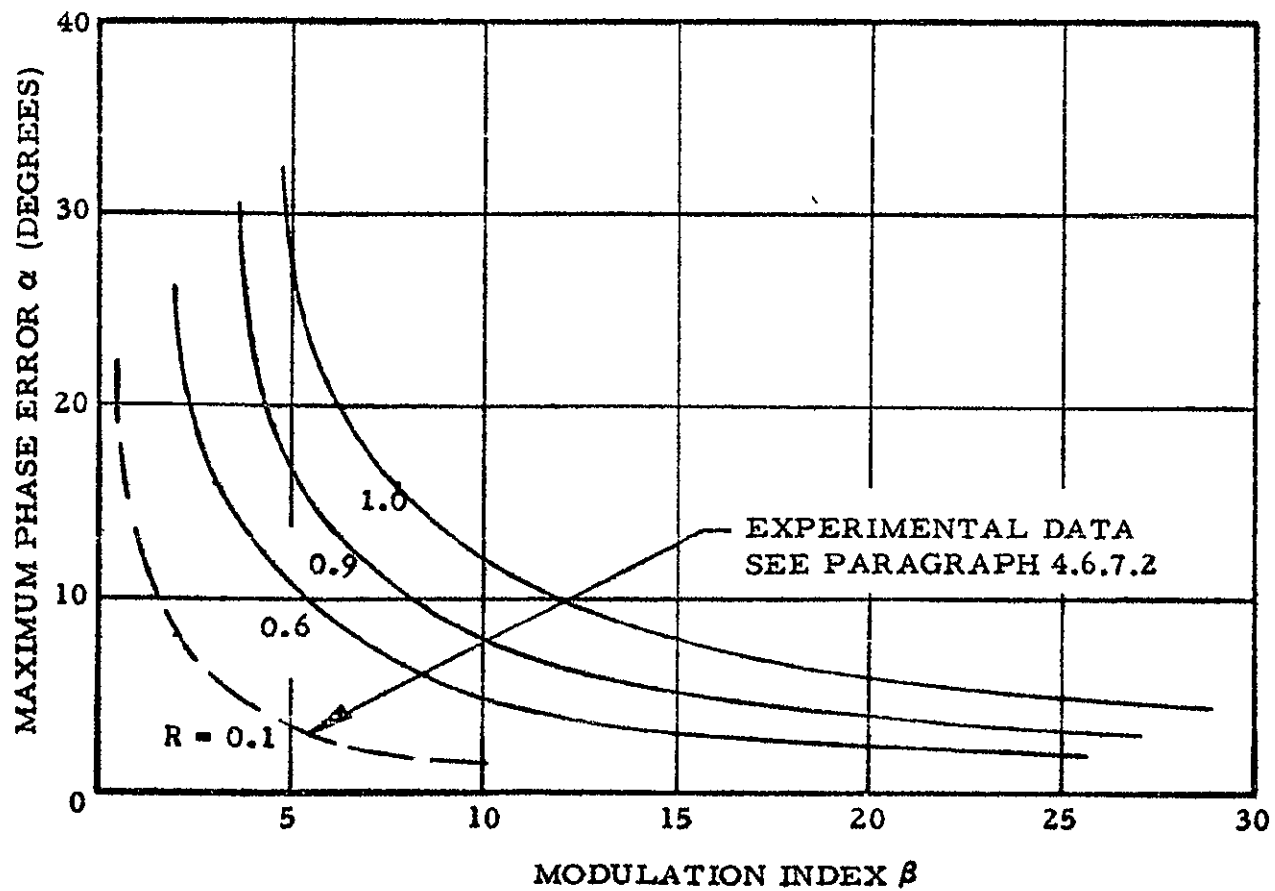
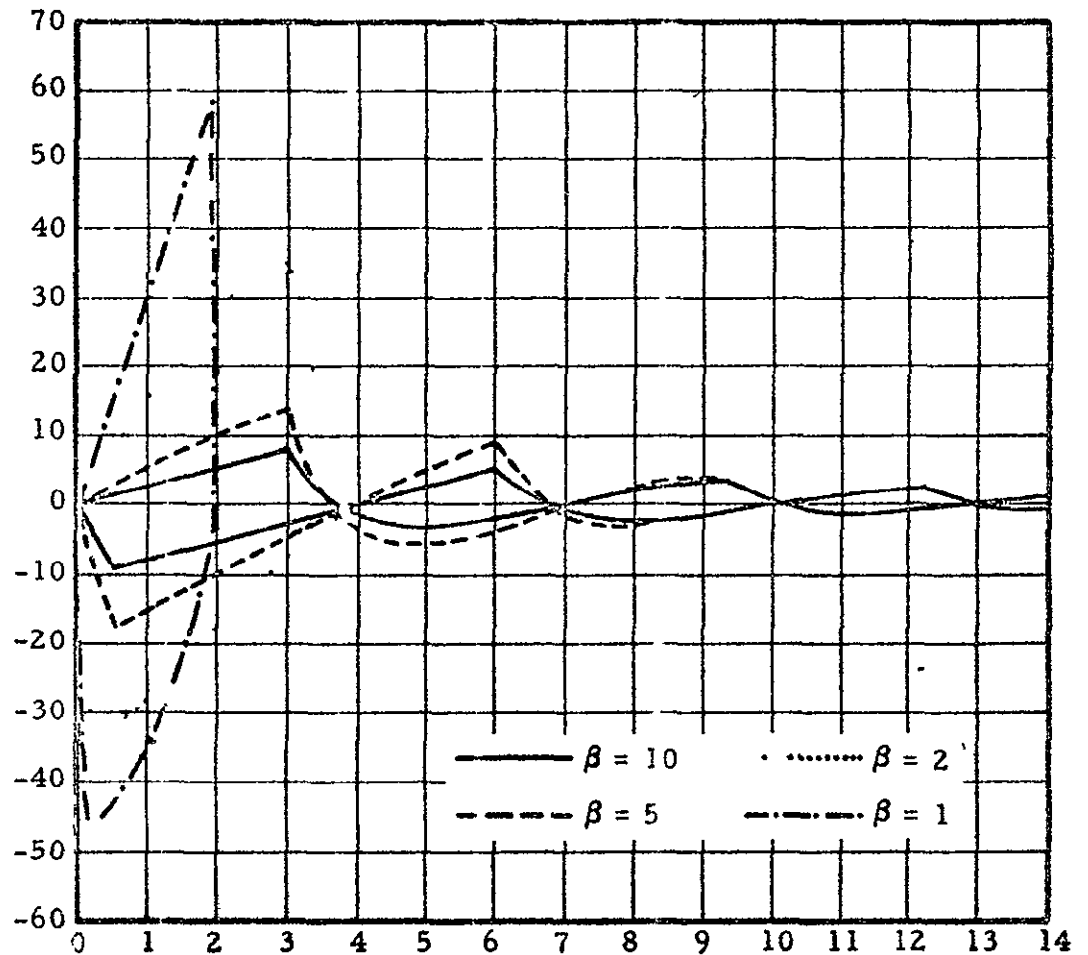


Figure 4 Maximum Phase Error After Detection as a Function of Modulation Index for Various Values of the Reflection Coefficient

NOTE TAKEN FROM "GROUND-REFLECTION PHASE ERRORS OF CW-FM TRACKING SYSTEMS" BY T. E. SOLLENBERGER,



β = MODULATION INDEX

R = REFLECTION COEFFICIENT = 0.9

$$Z = 2\beta \sin\left(\frac{\omega_m X}{\omega_c 2}\right)$$

Figure 5 Phase Error Envelope as a Function of Z

oscillation of Z ($\frac{\omega_m X}{\omega_c 2}$ varies from 0 to $\frac{\pi}{2}$ and Z progresses from 0 to 2β) and was obtained by using the values of C_0 from figure 2. When $\frac{\omega_m}{\omega_c}$ is known, α can be plotted versus X and this is shown in figure 6 for $\frac{\omega_m}{\omega_c} = 2(10^{-4})$. Note that this graph shows only the envelope as a function of X and does not show the fast oscillations. This curve can be used to determine typical values of α for particular geometrical situations as X is related to path delay through:

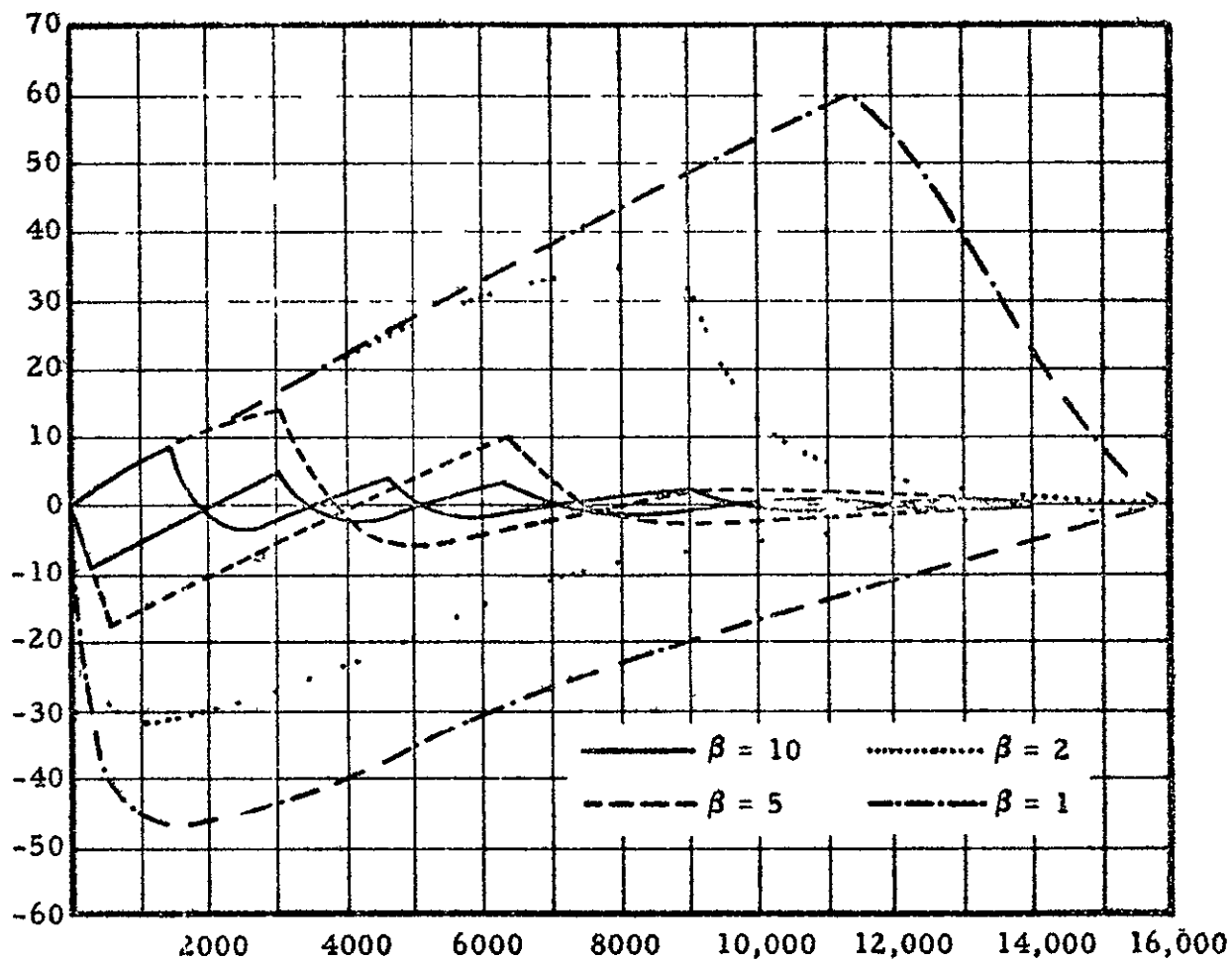
$$X = \omega_c t_d$$

Figures 4, 5, and 6 indicate that the phase error can be reduced by increasing the modulation index. This is an extremely important conclusion. Additional computations for α can be made with β fixed and R as a variable, producing a family of curves of α versus Z similar to figure 5. Plotting the peak of each curve yields figure 7 which indicates the variation of α with R for a fixed modulation index ($\beta = 10$).

It is interesting to observe what happens to α when R becomes 1. It can be shown that $\alpha = \frac{\omega_m t_d}{2}$ when $R = 1$ which means that α changes from an oscillating function for values of R slightly less than 1 to a linearly increasing angle equal to half the phase delay of the indirect propagation path at $R = 1$. Obviously, when $R < 1$ the receiver will not track the desired signal.

Multipath Effects on DME's The previous discussion has indicated that the phase shift due to multipath is dependent on the modulation index, reflection coefficient, and path delay of the indirect signal. In particular, it can be seen that a considerable reduction of phase error is achieved by using a modulation index of 10 or greater.

NOTE: TAKEN FROM "GROUND-REFLECTION PHASE ERRORS OF CW-FM TRACKING SYSTEMS" BY T. E. SOLLENBERGER



β = MODULATION INDEX

$$X = \omega_m t_d$$

R = REFLECTION COEFFICIENT = 0.9

$$\frac{\omega_m}{\omega_c} = 2(10^{-4})$$

Figure 6. Phase Error Envelope as a Function of X

NOTE: TAKEN FROM "GROUND-REFLECTION PHASE ERRORS OF CW-FM TRACKING SYSTEMS" BY T. E. SOLLENERGER

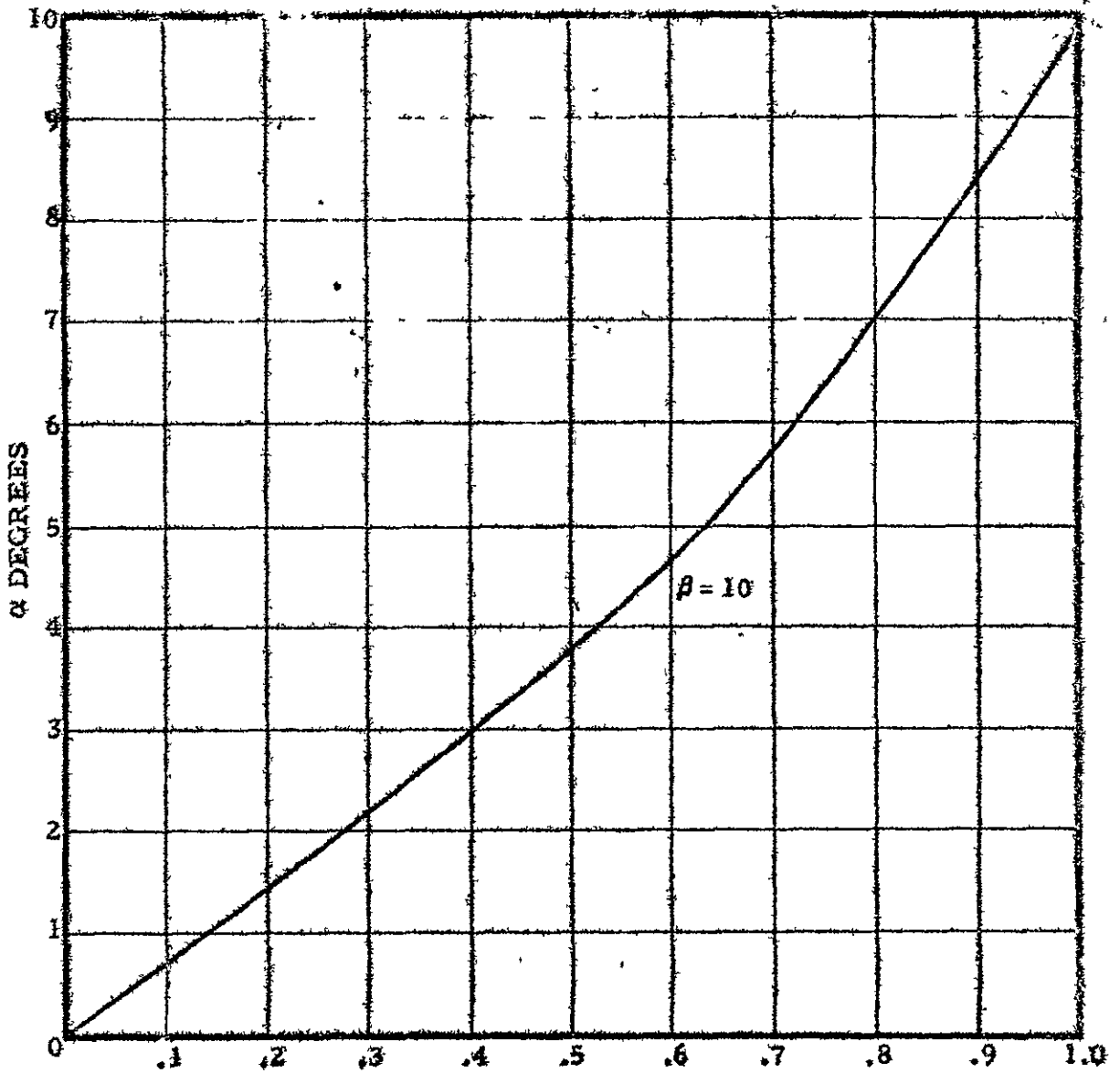


Figure 7. Phase Error at the First Maximum of the Phase Error Envelope as a Function of Reflection Coefficient

CUBIC CORPORATION
San Diego, California

24 June 1971

REVISIONS TO APPENDIX B OF
MID-STUDY REPORT ITR16-1
TROPOSPHERIC AND IONOSPHERIC PROPAGATION
EFFECTS ON RANGE MEASUREMENT DATED 22 MARCH 1971

The discussion of tropospheric and ionospheric propagation effects on range and range rate measurements dated 22 March 1971 and presented in the Mid-Study Report as Appendix B requires revision to account for results obtained from further investigation

It was discovered that the data for a constant range of 1 nautical mile, Tracking Geometry Case 2, was actually computed for a constant range of 2 nautical miles, so that all references to this case should be changed to read 2 nautical miles. The error previously reported as 900 ppm is actually 380 ppm, and the corrected error is 38 ppm. All copies dated 22 March 1971 should be corrected to reflect this change.



CUBIC
CORPORATION

22 March 1971
Revised 24 June 1971

1

APPENDIX B
TROPOSPHERIC AND IONOSPHERIC PROPAGATION
EFFECTS ON RANGE MEASUREMENT

by

Fred Lisenbe
Carl Mehr
Cubic Corporation

I PURPOSE

This paper presents approximations of atmospheric propagation effects on slant-range measurements produced by distance measuring equipment (DME) operating in the 1.5 - 2.25 GHz frequency range.

II TRACKING GEOMETRY

Two tracking situations were considered

Case 1 -- Vehicle in a 250 nm circular orbit at elevation angles between 5 and 90 degrees.

Case 2 -- Vehicle near the ground station at elevation angles between 5 and 90 degrees

For each elevation angle of the second case the refraction effects were computed for slant ranges of 2, 5, and 10 nautical miles

III MATHEMATICS

The propagation effects were computed from empirical correction equations that have been successfully employed for the correction of DME data from actual tracking systems such as ADAM and Azusa. These equations are discussed in detail in References 1, 2 and 3.



The empirical equations utilized by Cubic require minimum computations and meteorological and ionospheric electron density data for their operation. As stated in Reference 1, these corrections are accurate to within 10% for the troposphere and within 20% for the ionosphere.

A Tropospheric Refraction

The retardation in range due to propagation in the lower atmosphere is given approximately by

$$\Delta R = \frac{K_1 (1 - e^{-GH})}{\sin E_o + K_2 \cos E_o}$$

$$H = (R^2 + R_e^2 + 2RR_e \sin E_o)^{1/2} - R_e$$

where

- R = slant range in feet
- $K_1 \approx 8.5$ ft -- the tropospheric refraction at zenith
- $K_2 \approx 0.0236$ -- a control constant to compensate for round earth
- G = 1/ (22500 ft) a control constant for refraction in the troposphere
- H = altitude in feet
- R_e = radius of the earth in feet
- E_o = incident elevation angle

B Ionospheric Refraction

Retardation on ranging derived from frequency modulation

is given by

$$\Delta R = \frac{1325 H_o M_{F2}}{f^2 (0.05 \cos E_o + \sin E_o) W} \left\{ \tan^{-1}(W) - \tan^{-1} \left[\frac{(H_o - H) W}{H_o} \right] \right\} \left(1 - e^{-(H/160000)} \right)$$

where

H_o = Height of M_{F2} layer in feet (725000 used in model)

M_{F2} = maximum electron density in the F_2 layer of the ionosphere in electrons/ft³ (used 13.4987×10^9)

f = carrier frequency in cycles/sec

$W = \frac{2 H_o}{(H_H - H_L)}$ - - - control constant

H_H, H_L = upper and lower heights in feet of the half values of the electron density profile
(Used 1368600 and 608266, respectively in model)

IV RESULTS

The equations presented in Section III were implemented on a digital computer for the cases described in Section II

1 Case 1

a Total Propagation Effect

The tropospheric and ionospheric propagation effects were computed for the 250-nm orbit, for elevation angles between 5 and 90 degrees. The change in path lengths due to these effects are plotted in Figures 1 and 2. The relatively large range errors below 15° of elevation were not plotted in Figure 2 to allow greater resolution in the range error scale. The accuracy of the models allow correction of 90% of the tropospheric and 80% of the ionospheric effect. The residual errors after correction are plotted in Figure 3. If the residual error is considered to be a 3-sigma uncertainty in the correction, then the 3-sigma uncertainty of the total correction is the RMS of the individual uncertainties. This curve is also plotted in Figure 3. The slant range as a function of elevation angle is shown in Figure 5 for a 250 nm circular orbit.

b Frequency Effect

Inspection of the equation in Section III for the ionospheric model reveals that the increase in path length is inversely proportional to the square of the carrier frequency. This is demonstrated in the plot in Figure 4.

2 Case 2

The tropospheric refraction effect at "short" ranges as a function of elevation is shown in Figure 6. The flat earth model was considered to be appropriate at short ranges so the constant K_2 in the tropospheric refraction model was set equal to zero. When the accuracy is expressed in parts per million (ppm), the largest error plotted occurs at a range of 2 nm and 5° of elevation (380 ppm). The smallest error occurs at a range of 10 nm and 90° of elevation (130 ppm). Assuming that the refraction model is accurate to 10%, the maximum and minimum errors are reduced to 38 ppm and 13 ppm, respectively, by correction.



V COMMENTS

The data presented in this paper is intended to provide insight into the magnitude of the propagation effects. The data was obtained from empirical models utilized successfully in actual tracking systems. The ionospheric model utilized does not account for many of the physical phenomena that affect propagation in the ionosphere, such as diurnal variation, magnetic latitude variation, seasonal variation, and solar activity variation.

The Geodetic SECOR program, performed by Cubic for the Department of the Army, Corps of Engineers (references 3 and 4), provided an abundance of tracking data for which the ionospheric refraction effects could be computed directly from the multiple frequencies utilized in the tracking equipment.

A refined ionospheric refraction model was formulated by Cubic under contract to the U S Army Topographic Command (reference 5). The approach used was to identify the significant parameters affecting the magnitude of the ionospheric refraction, determine the functional dependence of refraction upon each parameter using results of the physics of the ionosphere tempered by empirical observations, and produce a single model whose parameters were determined using measured data.

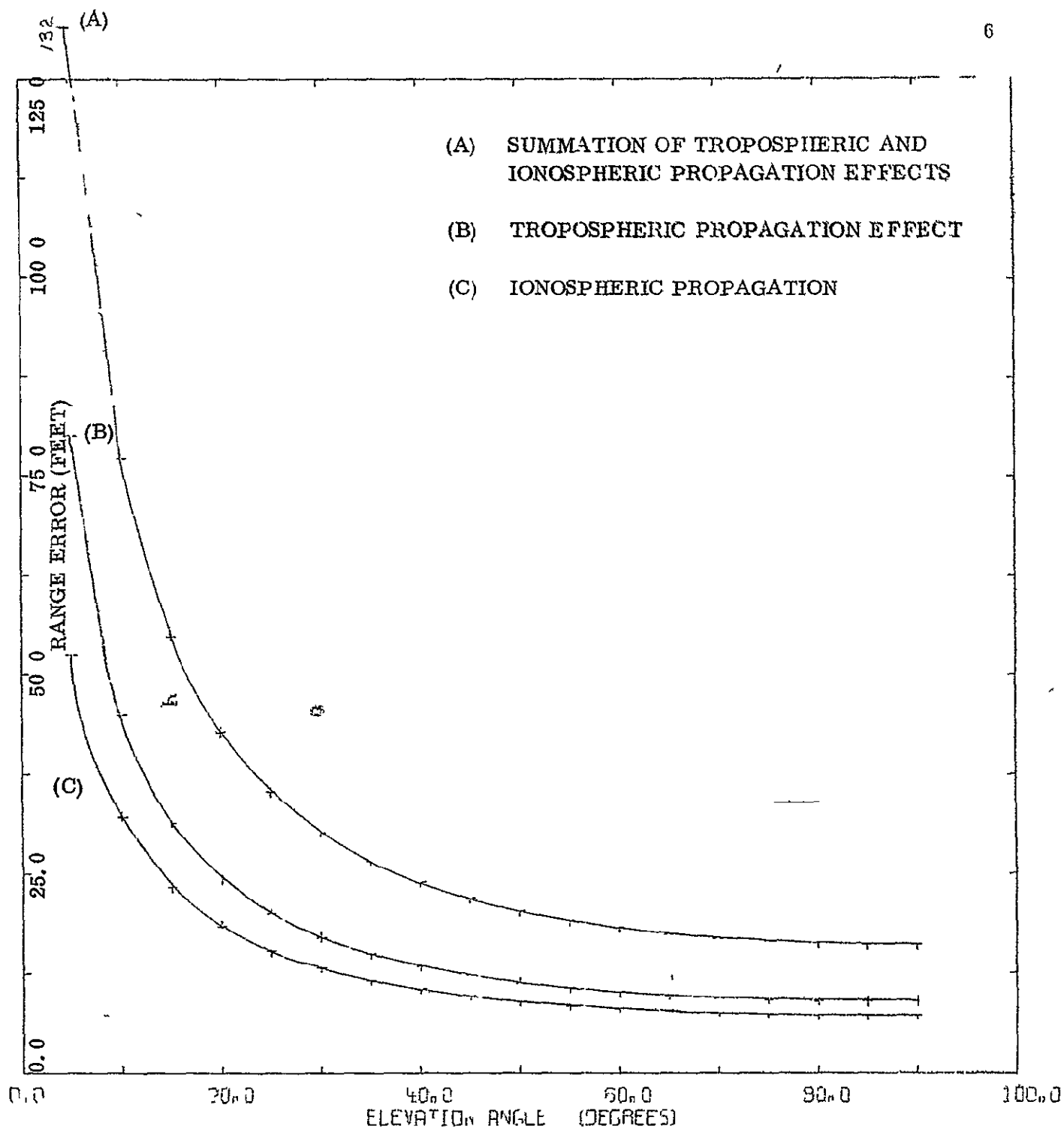
The higher frequencies to be employed by the proposed multilateration system for the space shuttle will significantly reduce the ionospheric effects from those observed by the SECOR equipment. The ionospheric refraction model to be used should be tailored specifically to the mission accuracy requirements of the space shuttle, and should be chosen based on the tradeoff of onboard computer requirements versus accuracy requirements.

It should be noted that the flat earth atmospheric refraction model degrades in accuracy below 5° of elevation angle, and should not be used below 2° of elevation.



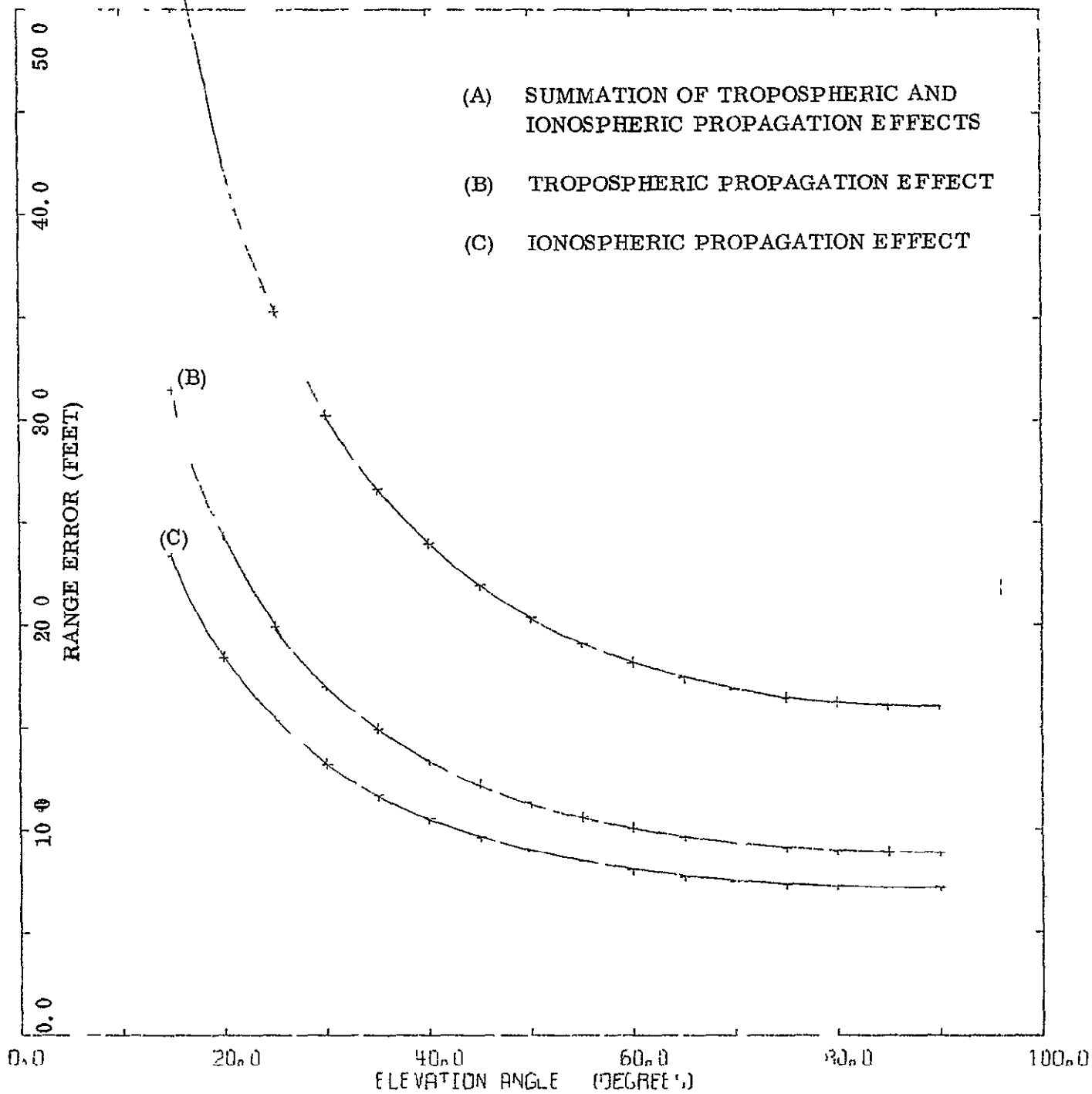
VI REFERENCES

- 1 Operation Fishbowl, Cubic Corporation Final Engineering Report, July 1963 (ADAM System)
- 2 Processing and Analysis of Azusa Mk II Data, Convair Astronautics Report No AE60-0117, June 1960
- 3 Mathematics of Geodetic SECOR Data Processing, Cubic Corporation Final Technical Report, September 1964
- 4 Mathematics for Army Map Service Geodetic Satellite Processing System, Cubic Corporation Final Technical Report, July 1968
- 5 Ionospheric Model Refinement, Cubic Corporation Technical Memorandum, August 1969



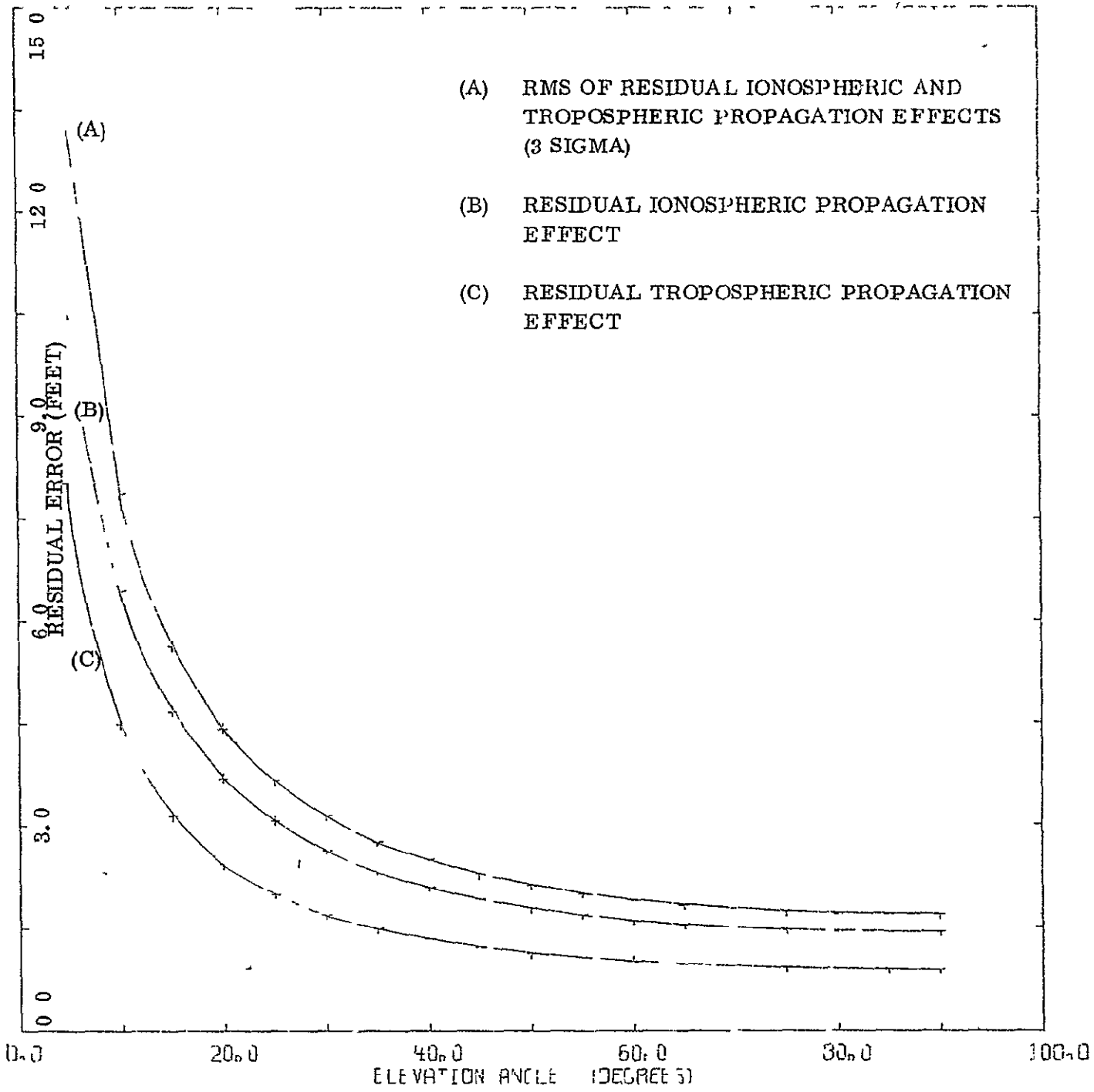
UNCORRECTED RANGE ERRORS DUE TO PROPAGATION EFFECTS FOR A CARRIER FREQUENCY OF 1.5 GHz AT AN ALTITUDE OF 250 N.M.

FIGURE 1



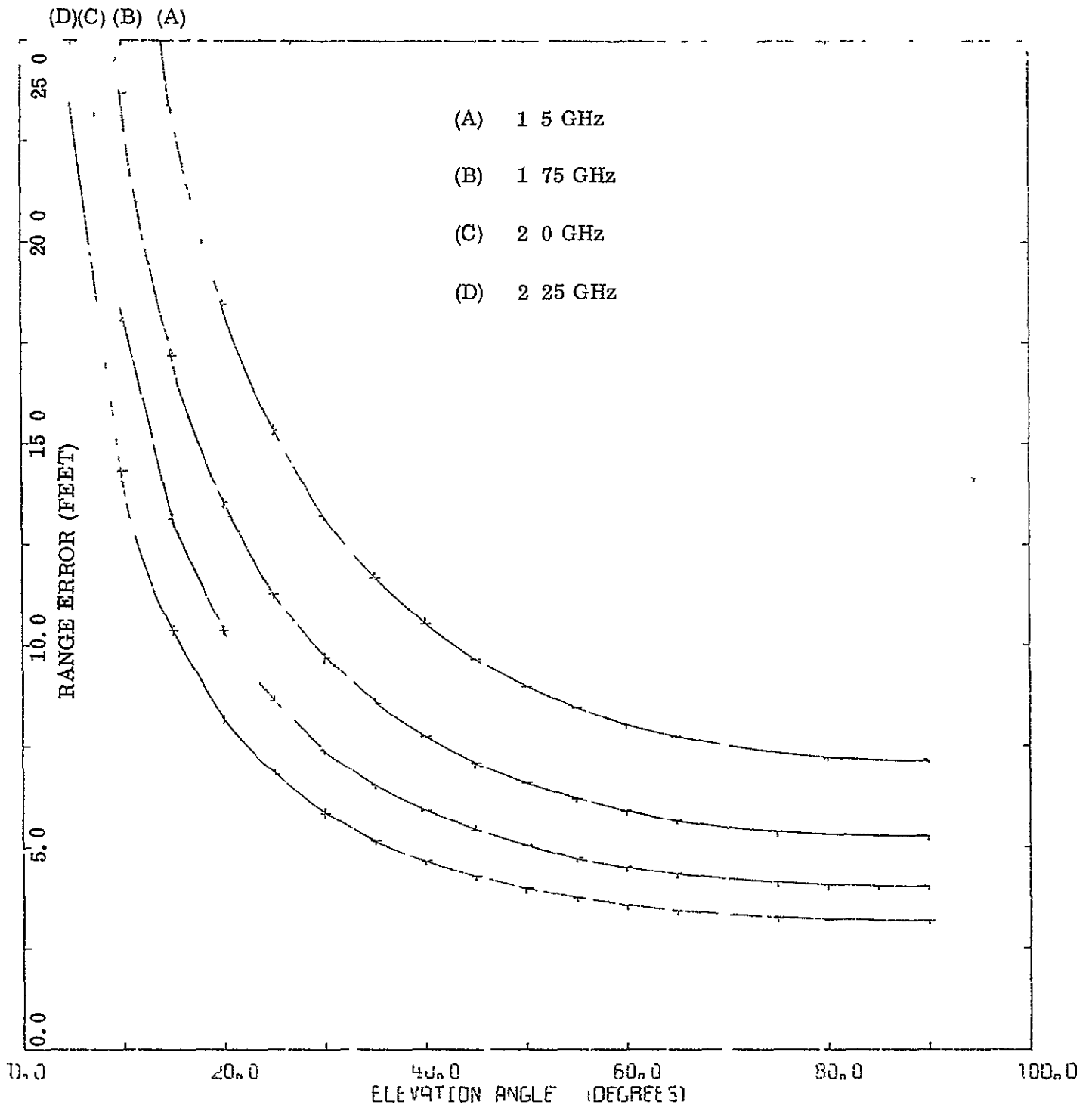
UNCORRECTED RANGE ERRORS DUE TO
 PROPAGATION EFFECTS FOR A CARRIER
 FREQUENCY OF 1.5 GHz AT AN ALTITUDE
 OF 250 N.M.

FIGURE 2



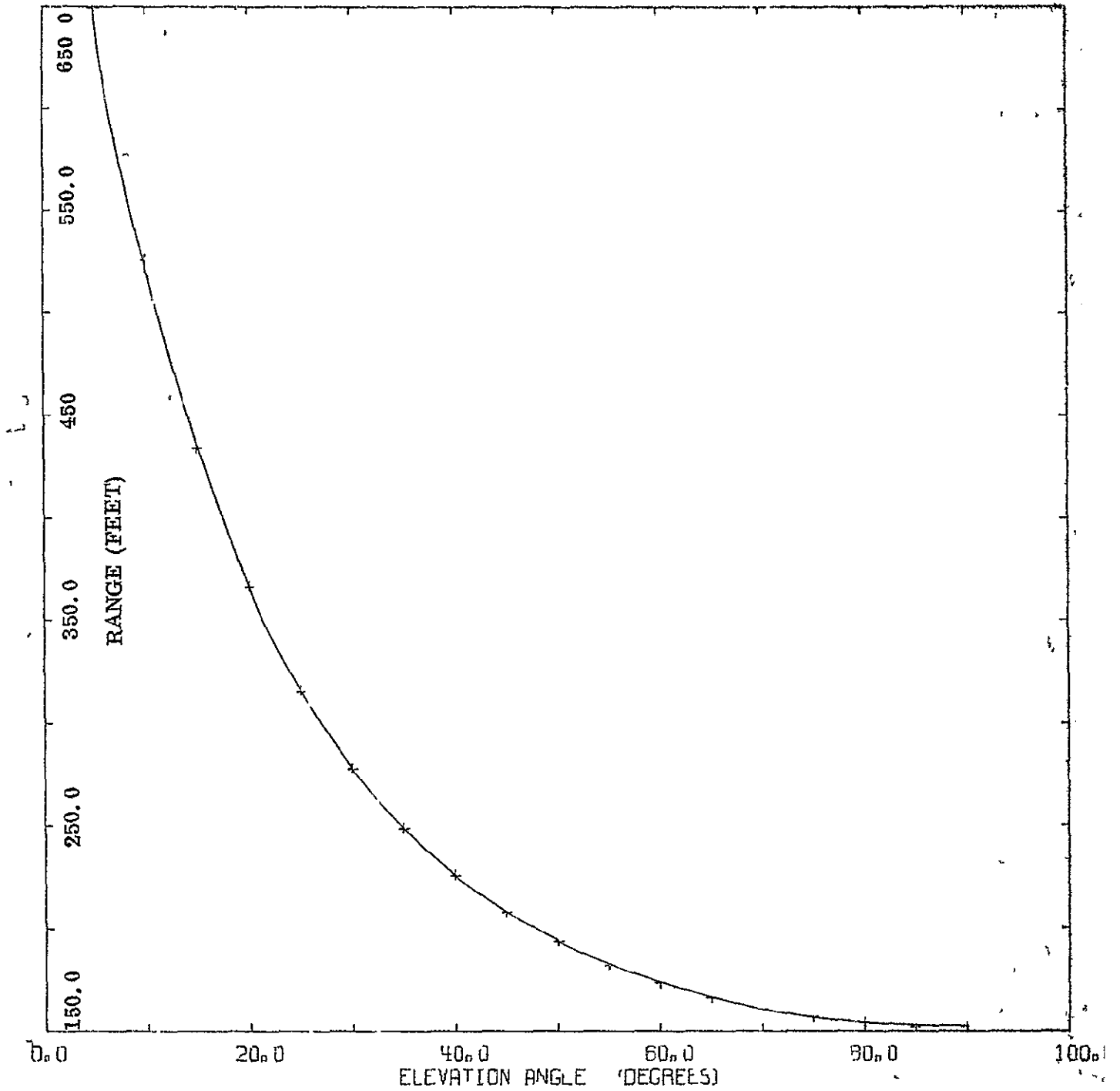
RESIDUAL RANGE ERRORS DUE TO PROPAGATION EFFECTS FOR A CARRIER FREQUENCY OF 1.5 CHZ AT AN ALTITUDE OF 250 N.M.

FIGURE 3

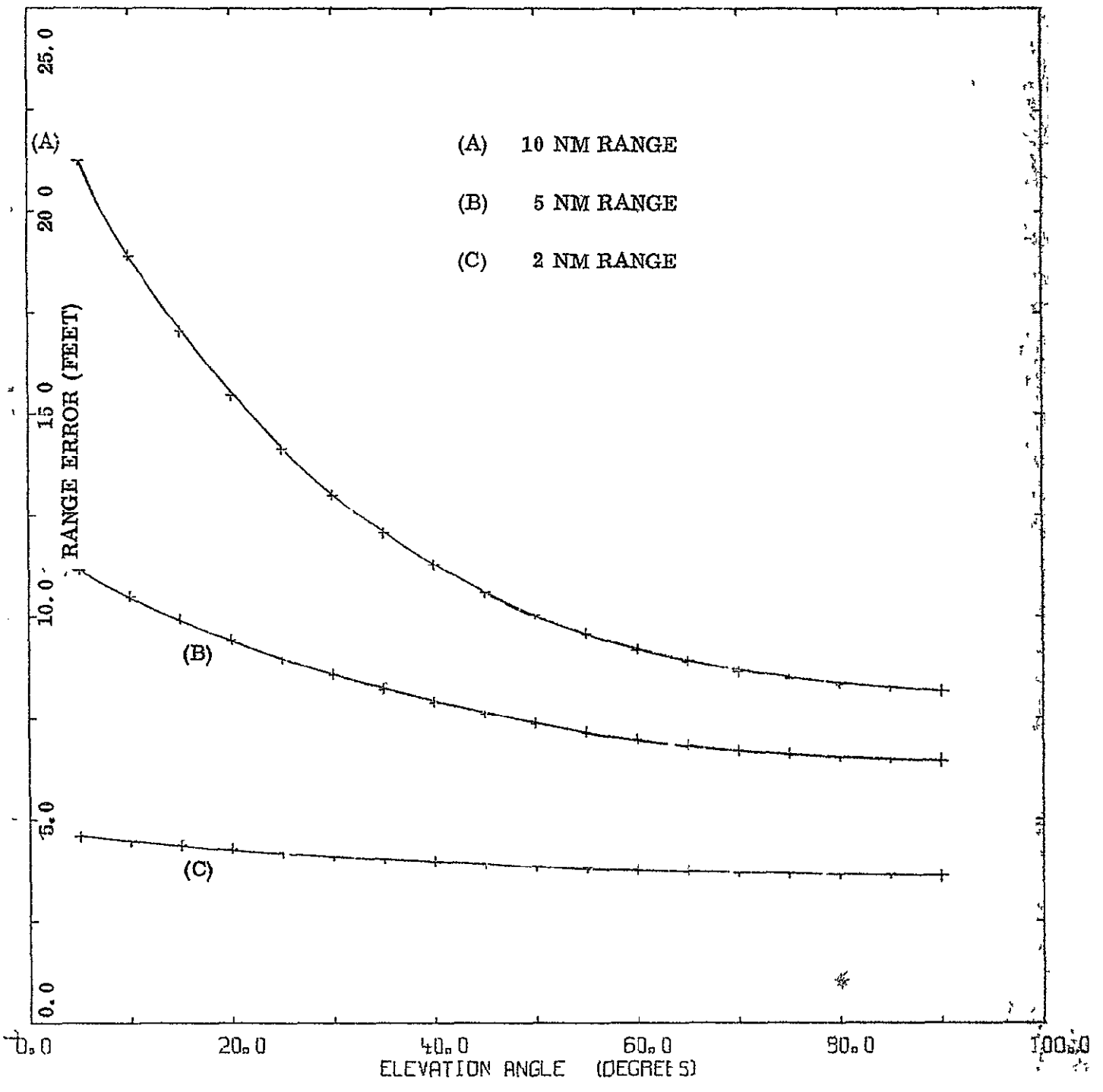


UNCORRECTED IONOSPHERIC RANGE ERRORS
 DUE TO PROPAGATION EFFECTS FOR
 VARIOUS CARRIER FREQUENCIES AT AN
 ALTITUDE OF 250 N.M.

FIGURE 4



RANGE AS A FUNCTION OF ELEVATION ANGLE
FOR A CONSTANT ALTITUDE OF 250 N.M.



UNCORRECTED RANGE ERRORS DUE TO TROPOSPHERIC PROPAGATION EFFECTS FOR VARIOUS CONSTANT RANGES

FIGURE 6

CUBIC CORPORATION
San Diego, California

24 June 1971

REVISIONS TO APPENDIX C OF
MID-STUDY REPORT ITR16-1
TROPOSPHERIC PROPAGATION EFFECTS
ON RANGE RATE MEASUREMENTS
DATED 4 MAY 1971

In the calculations of the range rate atmospheric error, the sign for the second term in the equation for ΔR should have been negative. This sign error caused the large discontinuity previously shown in the plot for the landing flight path, and Figure 4 is the corrected plot included in the revised report. The error quantities previously reported in terms of parts per million were based on a ratio of the range rate error to the horizontal velocity. These values have been recomputed based on a ratio with slant range rate. All copies dated 4 May 1971 should be corrected to reflect these changes.

CUBIC CORPORATION
San Diego, California

LAB
4 May 1971
Revised 24 June 1971

APPENDIX C

TROPOSPHERIC PROPAGATION EFFECTS

ON RANGE RATE MEASUREMENTS

I. PURPOSE

This paper presents approximations of tropospheric refraction effects on range rate measurements

II TRACKING GEOMETRY

Two cases were considered

Case 1

- A Range rate errors were computed as a function of elevation angle for a constant altitude of 30,000 feet for a target moving at a constant velocity of 550 feet/second
- B As above for an altitude of 15,000 feet and a velocity of 425 feet/second

Case 2

Range rate errors were computed as a function of ground distance for a landing profile. This approach trajectory was started at an altitude of 4,000 feet with a horizontal velocity of 200 knots and a glide slope of 12 degrees before flare. After flare, which occurred at an altitude of 775 feet, the horizontal velocity and glide slope were changed instantaneously to 175 knots and 3 degrees, respectively. The point of touchdown occurred at down range distance of 5,000 feet

Appendix C (Continued)

III Mathematics

The range rate measurements were obtained from differencing two range measurements taken at a different time, such that

$$R \text{ meas} = \frac{R \text{ meas}_2 - R \text{ meas}_1}{\Delta t}$$

$$R \text{ meas}_2 = (R_{T2} + \Delta R_2)$$

$$R \text{ meas}_1 = (R_{T1} + \Delta R_1)$$

where

$$R_{T1}, R_{T2} = \text{True range at time } T_1, T_2$$

$$\Delta R_1, \Delta R_2 = \text{Refraction error in measured range at time } T_1, T_2$$

substituting yields

$$\begin{aligned} R \text{ meas} &= \frac{(R_{T2} + \Delta R_2) - (R_{T1} + \Delta R_1)}{\Delta t} \\ &= \frac{(R_{T2} - R_{T1})}{\Delta t} + \frac{(\Delta R_2 - \Delta R_1)}{\Delta t} = R_T + \Delta R \end{aligned}$$

where

ΔR is the time rate of change of range refraction error

The error in measured range due to tropospheric refraction effects is given by

$$\Delta R = \frac{K_1 (1 - e^{-GH})}{\sin E_0 - K_2 \cos E_0}$$

$$H = (R^2 + R_e^2 + 2RR_e \sin E_o)^{1/2} - R_e$$

where

R = slant range in feet

$K_1 \approx 8.5$ ft -- the tropospheric refraction at zenith

$K_2 \approx 0.0236$ -- a control constant to compensate for round earth

G = $1/(22500$ ft) a control constant for refraction in the troposphere

H = altitude in feet

R_e = radius of the earth in feet

E_o = incident elevation angle

Range rate error is approximated by the time derivative of ΔR for the center point of the time interval defined by T1 and T2

Assuming the flat earth model, this derivative is

$$\dot{\Delta R} = \frac{K_1 G H e^{-GH}}{\sin E_o} - \frac{\dot{E}_o}{\tan E_o} \Delta R$$

where

H = altitude rate in feet/second

\dot{E}_o = angular rate of incident elevation angle

IV RESULTS

The equation presented in Section III for range rate error was implemented on a digital computer for the cases described in Section II. The accuracy of the model allow correction of 90% in the range rate error. The corrected range rate is defined as

$$\dot{R}_c = \dot{R}_{meas} + \Delta \dot{R}$$

when R_{meas} is negative, ΔR is positive and when R_{meas} is positive, ΔR is negative (i.e., the net effect of correction is to decrease the magnitude of the measured range rate, R_{meas})

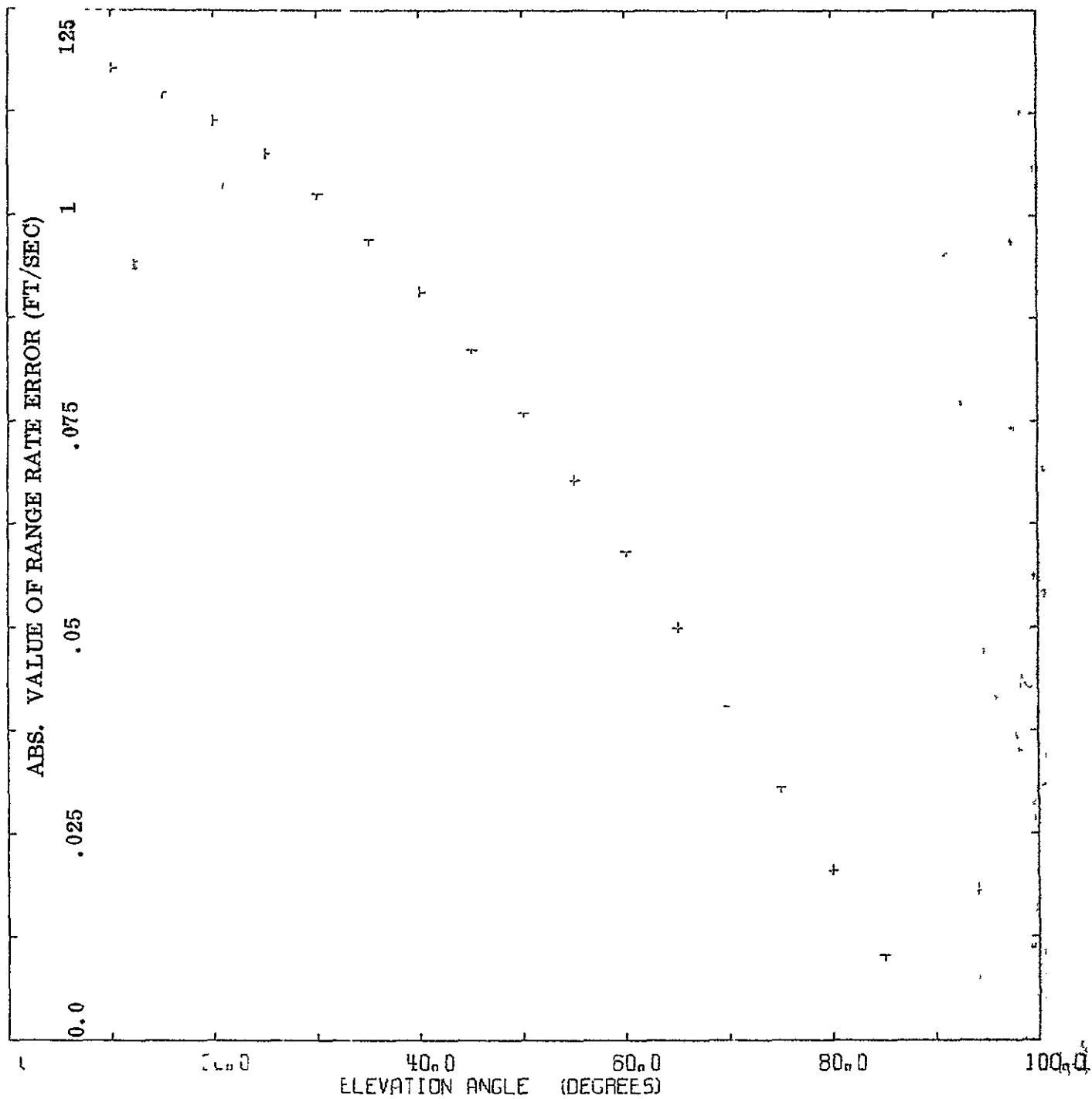
Case 1

Figures 1 and 2 show the expected range rate errors as a function of elevation angle for constant altitudes of 30,000 and 15,000 feet, respectively. When the accuracy of the model is expressed in parts per million (ppm), the following results are obtained:

- a The 30,000 feet of altitude case yields a corrected range rate of approximately 21.5 ppm at 85 degrees of elevation and 22.4 ppm at 5 degrees of elevation.
- b The 15,000 feet of altitude case yields a corrected range rate of approximately 28.3 ppm at 85 degrees of elevation and 29.3 ppm at 5 degrees of elevation.

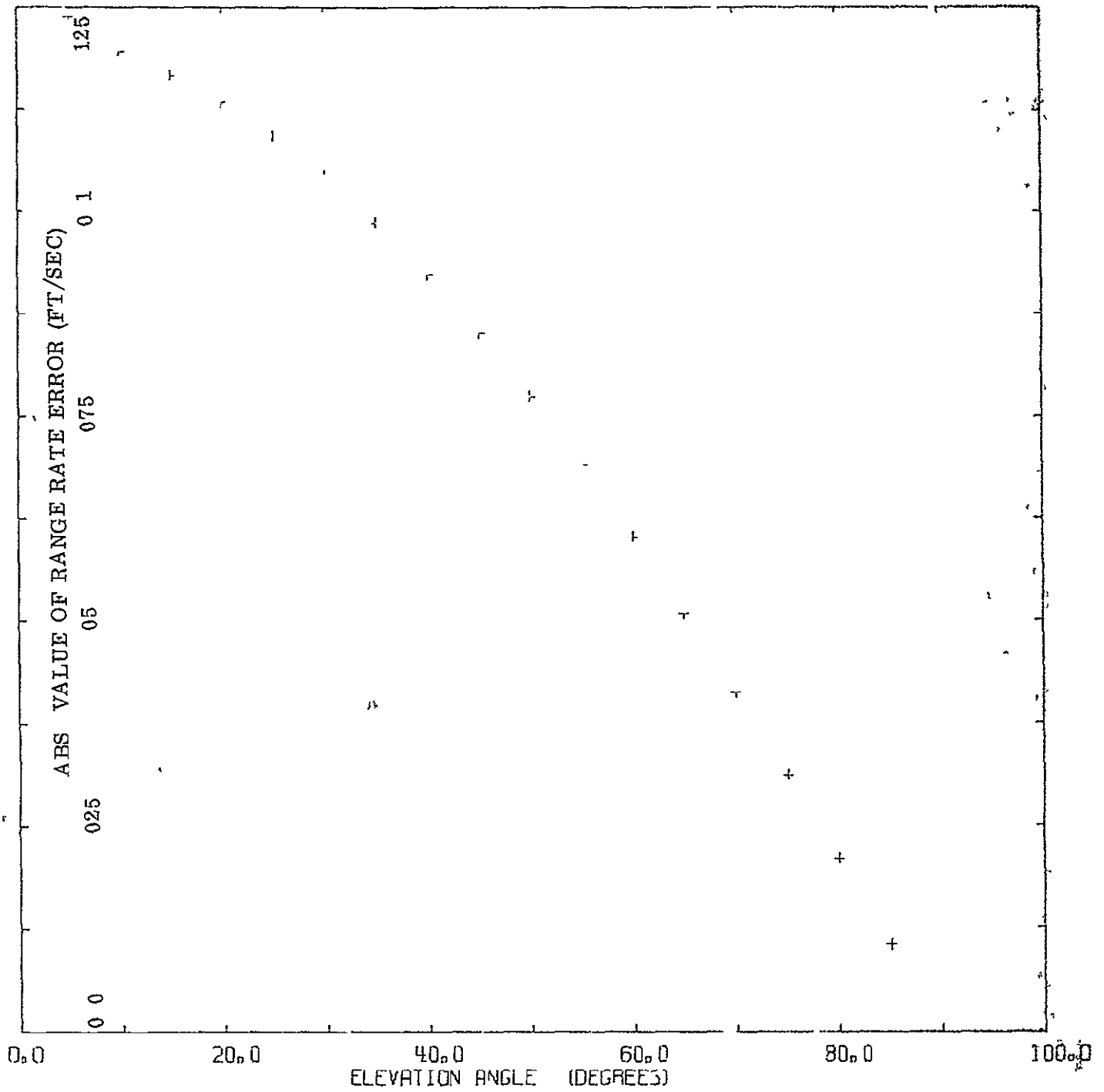
Case 2

The landing flight path shown in Figure 3 yielded range rate errors as shown by Figure 4. The DME station is located at the lower left corner of Figure 3.



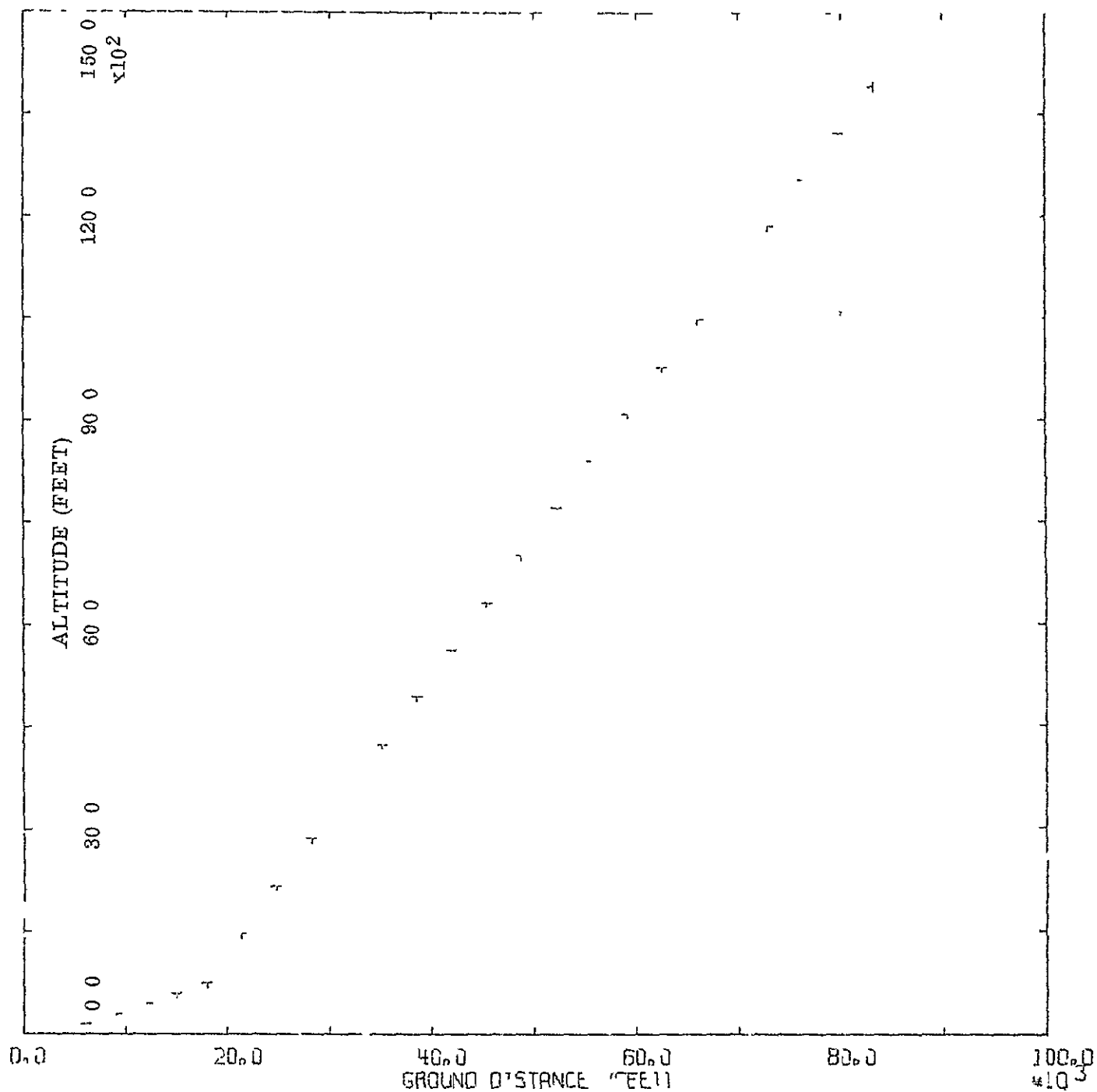
RANGE RATE ERRORS AS A FUNCTION OF
ELEVATION ANGLE FOR A CONSTANT ALTITUDE
OF 30000 FEET WITH A SPEED OF 550 FT/SEC

FIGURE 1

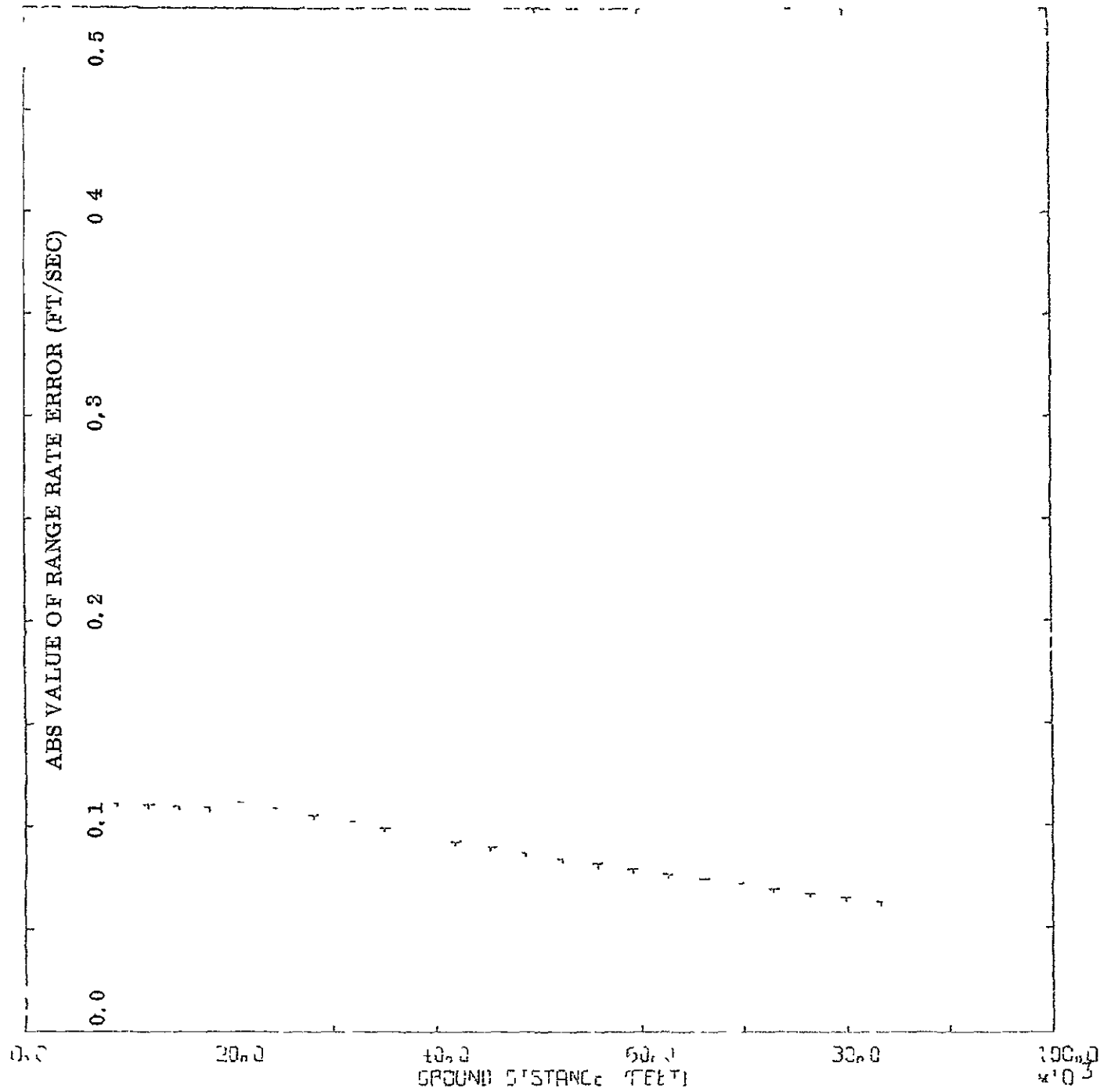


RANGE RATE ERRORS AS A FUNCTION OF
ELEVATION ANGLE FOR A CONSTANT ALTITUDE
OF 15000 FEET WITH A SPEED OF 425 FT/SEC

FIGURE 2



LANDING FLIGHT PATH, HORIZONTAL VELOCITY
 BEFORE FLARE 200 KNOTS, AFTER FLARE 175
 KNOTS, CLIDE SLOPE 12 DEGREES BEFORE
 FLARE, AFTER FLARE 3 DEGREES.



RANGE RATE ERRORS AS A FUNCTION OF
GROUND DISTANCE FROM DME STATION FOR THE
LANDING FLIGHT PATH.

FIGURE 4

APPENDIX D

SECTION II - ' EVALUATION OF
SHIRAN GEODETIC SURVEYING "

FROM

SHIRAN

GEODETIC SURVEY SYSTEM ELECTRONIC

AN/USQ-32(XA-1)

FLIGHT TEST AND EVALUATION PROGRAM REPORT

CUBIC CORPORATION

TECHNICAL REPORT SEG-TDR-64-53

APRIL 1965

SYSTEM ENGINEERING GROUP
RESEARCH AND TECHNOLOGY DIVISION
AIR FORCE SYSTEMS COMMAND
WRIGHT-PATTERSON AIR FORCE BASE, OHIO

SECTION II

EVALUATION OF SHIRAN GEODETIC SURVEYING

2 1 Introduction Geodetic surveying by aerial electronic technique relies on the ability of the system to measure geodetic distances between widely separated ground locations to map standard accuracies. A least squares adjustment of these distances, 1 e , of the trilateration network, then establishes the geodetic positions of the ground station locations. The accuracy of the SHIRAN system in performing line measurements over land and water and at varying altitudes was evaluated and comprehensive analyses of various network adjustments were made. The evaluation was divided into the following phases:

- 1 Comparison of SHIRAN and Geodetic Distances,
- 2 Network Adjustment and Constant Errors,
- 3 Overwater Test, and
- 4 Repeatability Test (multialtitude line crossings Catalina-Ajo Line)

2 2 Comparison of SHIRAN and Geodetic Distances Prior to the adjustment of the trilateration network, the twelve crossings of each line were averaged and evaluated for internal consistency. The deviations and PE_s for each line are given in Appendix II. The mean SHIRAN reduced value for each line was then compared with the computed inverse distance based on the ground survey positions. The geodetic positions of the six stations listed below were found by measuring the offset of the mast from the geodetic markers.

<u>STATION</u>	<u>CODE NAME</u>	<u>STATION MAST POSITION</u>	
		<u>LONGITUDE</u>	<u>LATITUDE</u>
		<u>o</u> <u>'</u> <u>"</u>	<u>o</u> <u>'</u> <u>"</u>
Gentry L O Tower	Gentry	110 42 45.231	34 18 05.285
Catalina 2 Reset	Cat	110 47 16.427	32 26 34.329
Ajo	Ajo	112 50 31.611	32 19 24.853
Quartz	Quartz	112 56 07.379	33 55 27.707
Hayford	Hayford	115 11 59.863	36 39 27.945
San Antonio	Antonio	117 14 31.707	38 18 31.288

The direct comparisons, which are shown in Table I, indicate SHIRAN-Geodetic accuracy and the existence of possible constant or systematic errors.

TABLE I
SHIRAN-GEODETIC DISTANCE COMPARISONS

<u>LINE</u>	<u>SHIRAN (N Miles)</u>	<u>GEODETIC (N Miles)</u>	<u>S-G x 10⁴ (N Miles)</u>
Cat-Gentry	111 3648	111 3673	-25
Ajo-Gentry	159 6634	159 6643	- 9
Ajo-Cat	104 6148	104 6172	-24
Quartz-Gentry	113 0140	113 0154	-14
Quartz-Cat	139 8666	139 8689	-23
Quartz-Ajo	95 9722	95.9754	-32
Hayford-Gentry	261 2550	261 2564	-14
Hayford-Cat	333 9010	333 9027	-17
Hayford-Ajo	284 6983	284 6971	+12
Hayford-Quartz	197 9326	197 9332	- 6
Antonio-Gentry	397 2113	397 2118	- 5
Antonio-Cat	472 7701	472 7712	-11
Antonio-Ajo	418 4664	418 4659	+ 5
Antonio-Quartz	335 8142	335 8151	- 9
Antonio-Hayford	138 9145	138 9171	-26
		MEAN =	-13

$$PE_s = 0.6745 \sqrt{\frac{\sum x^2}{N}}$$

$$PE_s = \pm 0.0012 \text{ N Mile}$$

$$x = (S-G)$$

2.2.1 Discussion of SHIRAN-Geodetic Errors Results of the SHIRAN-Geodetic comparisons before adjustment provide the first basis for evaluating SHIRAN-Geodetic accuracy. The PE_s of 0.0012 nautical mile is significantly less than the PE_s of 0.0017 nautical mile specified for a network adjustment. An analysis of the signs of the errors suggests the existence of a possible systematic or constant error in SHIRAN range measurements or the computed inverse. The signs of the errors are systematically negative (except for two) and the mean is -0.0013 nautical mile. The possibility of a constant error is discussed in greater detail in Paragraph 5.1.

2 3 Network Design The trilateration network was designed to yield optimum information on SHIRAN distance measuring consistency. Four sliver triangles were incorporated in the network to assist in providing a strong determination of any constant error. The sliver triangles involved 9 of the 15 lines in the network and included the four approximately co-linear stations CAT, QUARTZ, HAYFORD, and ANTONIO.

2.3.1 Internal Consistency. Depending on the constraints included in the network, adjustment information was obtained in specific areas of investigations. The free adjustment technique involves a minimum of constraints and provides information on the internal consistency of SHIRAN measurements, which is reflected in the probable error of a single measurement and the resulting residuals for each adjusted line. The differential formulae which relate variations in azimuth and length with variations in geographic position of the terminals of a geodetic line are given in Appendix III. The basic free adjustment employed was that where two coordinates of one station and only one coordinate of a second station were held fixed. Eight free adjustments were made with these constraints holding various combinations of coordinates fixed. The results of these basic free adjustments were identical in every case, i. e., the results were within 0.0001 nautical mile, no matter which station was held fixed. The maximum residual was 0.0019 nautical mile and the probable error of a single observation was ± 0.0011 nautical mile.

FREE ADJUSTMENT RESULTS

<u>LINE</u>	<u>RESIDUAL</u> <u>x 10⁴ (N Miles)</u>
Cat-Gentry	+ 6
Ajo-Gentry	- 12
Ajo-Cat	+ 4
Quartz-Gentry	+ 10
Quartz-Cat	+ 4
Quartz-Ajo	+ 19
Hayford-Gentry	+ 5
Hayford-Cat	+ 2
Hayford-Ajo	- 4
Hayford-Quartz	+ 16
Antonio-Gentry	- 7
Antonio-Cat	- 12
Antonio-Quartz	+ 8
Antonio-Hayford	+ 18
Antonio-Ajo	- 8

$$PE_s = \pm 0.0011 \text{ N. Mile}$$

The probable error of ± 0.0011 nautical mile is well within the basic specification of ± 0.0017 nautical mile established for the system's overall distance-measuring accuracy. In a second series of adjustments, the terminal points of a line and the included base length were held fixed. The adjustment technique was repeated for each of the lines in the network. The results for this series of adjustments are shown in Table II. Analysis of the PE_s for each of the base line adjustments again shows that the specification of ± 0.0017 nautical mile for the PE_s is satisfied in each case. These adjustments with one additional constraint also demonstrated the overall consistency of SHIRAN measuring accuracy.

2.3.2 Conclusions In all adjustments performed, SHIRAN accuracy satisfied the specification of 0.0017 nautical mile. The investigation of a constant error K (which is discussed in paragraph 5.1) showed that a constant error quantity does exist in the data and the magnitude is between 0.0010 and 0.0016 nautical mile. It should be noted that, with or without the incorporation of the K factor, the SHIRAN system accuracy remains within specifications. The inclusion of the K factor, however, appreciably reduces the adjustment residuals and the probable error of a single observation. The source of this constant error is not necessarily in the SHIRAN system but can be attributed to some combination of the following

- 1 Index of refraction error,
- 2 Altitude errors causing horizontal errors as a function of range, and/or
- 3 Systematic error in computed inverses

2.4 Overwater Test. The overwater test was performed to check the behavior of SHIRAN over a highly reflective surface and over widely varying geometries. The test consisted of the repeated measurement of a line 184 nautical miles in length at 2000 foot intervals from the minimum altitude of 4500 feet to a maximum altitude of 33,500 feet. The ground station sites selected for the overwater test were stations Point Loma, in the vicinity of San Diego, and Gaviota, in the vicinity of Santa Barbara.

<u>STATION</u>	<u>LONGITUDE</u>			<u>LATITUDE</u>		
	0	1	''	0	1	''
Gaviota	120	11	52 053	34	30	06 542
Point Loma	117	14	27 561	32	40	22 467

TABLE II
NETWORK ADJUSTMENTS HOLDING TWO STATIONS FIXED

Code Nos (1) Gentry L O Tower (3) Ajo (5) Hayford
(2) Catalina 2 Reset (4) Quartz (6) San Antonio

Residual = $V \times 10^4$ N Miles

Stations Fixed Line	1-2	1-3	1-4	1-5	1-6	2-3	2-4	2-5	2-6	3-4	3-5	3-6	4-3	4-6
Cat-Gentry	fixed	+13	+ 5	+ 5	+ 4	- 8	+ 7	+12	+15	+ 5	+ 6	+ 5	+ 5	+ 6
Ajo-Gentry	- 6	fixed	-11	-12	-12	- 6	-18	-16	-17	- 8	-13	-12	-13	-12
Ajo-Cat	- 3	+11	+ 4	+ 3	+ 3	fixed	+ 9	+ 7	+ 9	+ 4	+ 5	+ 3	+ 3	+ 4
Quartz-Gentry	+ 9	+15	fixed	+10	+11	+ 8	+17	+ 7	+ 6	+ 4	+ 9	+10	+11	-10
Quartz-Cat	+ 5	- 1	+ 5	+ 4	+ 4	+ 8	fixed	+12	+17	+ 5	+ 4	+ 4	+ 8	+ 4
Quartz-Ajo	+19	+25	+18	+20	+20	+19	+21	+18	+18	fixed	+17	+20	+24	+19
Hayford-Gentry	+ 3	+ 6	+ 5	fixed	+ 7	+ 3	+ 3	+11	+ 4	+ 7	+ 7	+ 5	+ 5	+ 5
Hayford-Cat	+ 6	- 1	+ 1	+ 4	+ 2	+ 4	+10	fixed	+15	+ 1	+ 5	+ 2	+ 2	+ 2
Hayford-Ajo	- 6	- 3	- 4	- 6	- 2	- 6	- 3	0	- 6	0	fixed	- 4	-10	- 4
Hayford-Quartz	+16	+17	+15	+16	+16	+17	+ 8	+22	+15	+11	+13	+15	fixed	+16
Antonio-Gentry	-10	- 6	- 7	- 5	fixed	- 9	- 9	- 8	+ 3	- 5	- 8	- 8	- 8	- 8
Antonio-Cat	- 8	-15	-13	-12	-10	-10	- 4	- 4	fixed	-13	-12	-12	-12	-12
Antonio-Ajo	-10	- 7	- 7	- 6	-11	-10	- 6	- 9	- 1	- 4	- 9	fixed	- 6	- 7
Antonio-Quartz	+ 9	+10	+ 8	+ 9	+ 9	+10	0	+ 8	+18	+ 4	+ 9	+ 9	+ 4	fixed
Antonio-Hayford	+19	+19	+18	+16	+22	-18	+18	+12	+28	+18	+19	+19	+22	+19
MEAN	+ 3	+ 6	+ 2	+ 3	- 4	+ 3	+ 4	+ 4	+ 9	+ 2	+ 3	+ 4	+ 2	+ 3
PE _s	+13	+13	+10	+11	+12	+11	+12	+12	+15	+ 8	+11	+11	+12	+11

AU-6

Results for the overwater tests flown 15 and 20 August 1963 are shown in Table III. Figure 2 shows the overwater test ΔN profiles.

TABLE III

RESULTS OF OVERWATER TESTS 15 and 20 AUGUST 1963
(Line Gaviota-Point Loma)

<u>LINE No.</u>	<u>ALTITUDE (Feet)</u>	<u>SHIRAN REDUCED (SR) N Miles</u>	<u>V = SR - MEAN SR ($\times 10^4$) N Miles</u>
<u>15 August 1963</u>			
1	25 964	184.2732	+ 1
2	34 508	184 2743	+12
3	32 237	184 2731	0
4	30 217	184 2731	0
5	28 188	184 2726	- 5
6	25 967	184.2717	-14
7	23 887	184 2711	-20
8	21 795	184 2743	+12
9	19 664	184 2727	- 4
10	15 476	184 2738	+ 7
11	13 275	184 2738	+ 7
12	11 132	184 2788	Rejected, Noise

MEAN SHIRAN = 184 2731 N Miles

 $PE_s = \pm 0.0007$ N Miles

Geodetic Distance = 184.2735 N Miles

20 August 1963

1	15 391	184 2748	+12
2	15 401	184 2720	-16
3	13 356	184 2738	+ 2
4	13 476	184 2755	+19
5	11 081	184 2706	-30
6	8 901	184 2561	Rejected, Noise
7	7 866	184 2767	+31
8	6 736	184 2677	Rejected, Noise
9	5 694	184 2739	+ 3
10	4 606	184 2717	-19
11	3 624	184.2668	Rejected, Noise

MEAN SHIRAN = 184.2736 N Miles

 $PE_s = \pm 0.0014$ N Miles

Geodetic Distance = 184.2735 N Miles

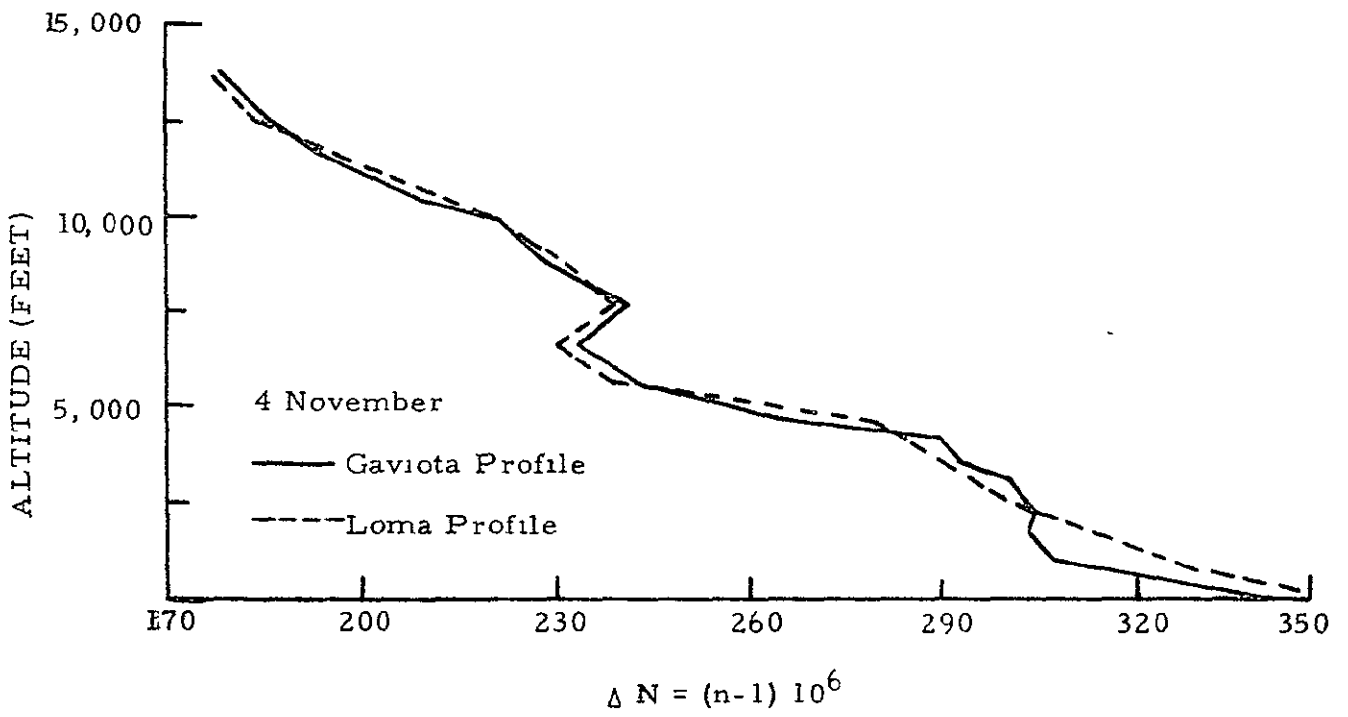
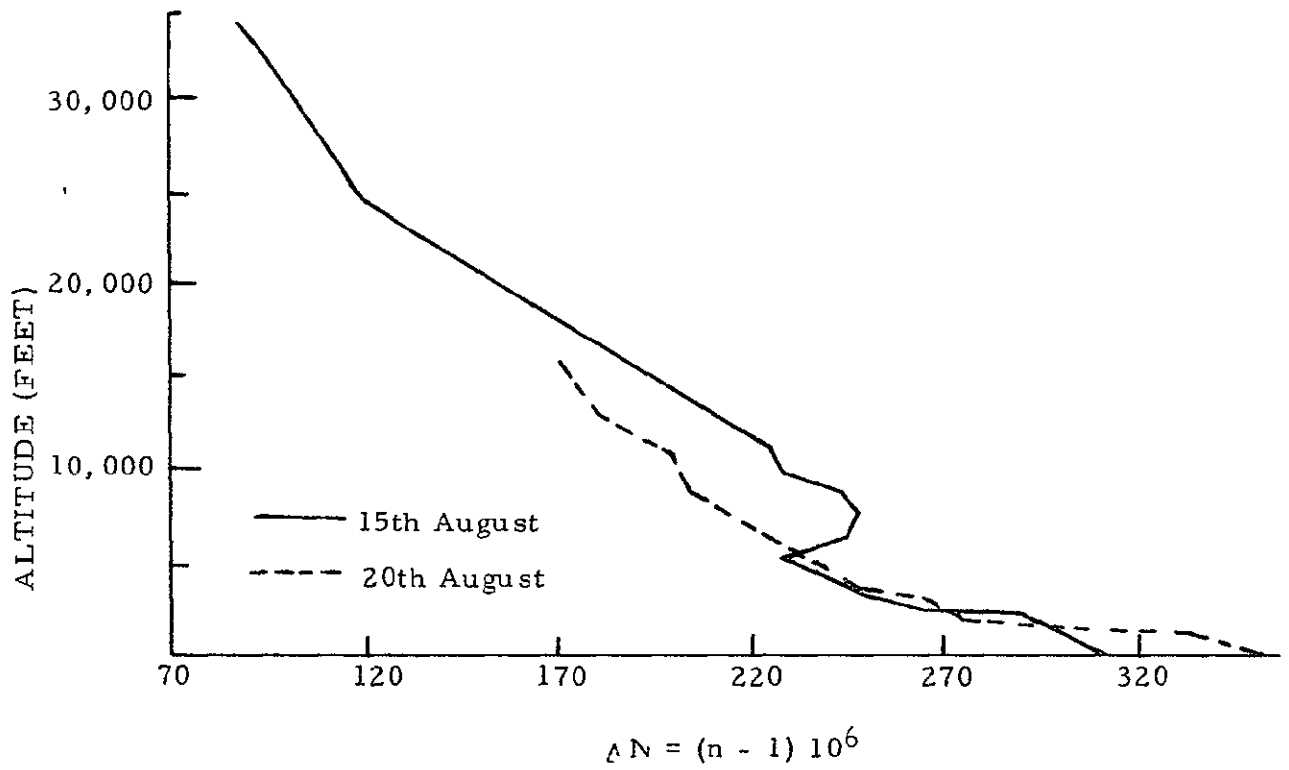


Figure 2 Overwater Test ΔN Profiles

2 4 1 Analysis of Overwater Test Results Results of the overwater test flights should be qualified due to the unusual refraction profile existing at the time of the tests. A prominent inversion (a 50 unit variation in 400 feet altitude) in the index of refraction profile apparently had an adverse effect on line crossings flown below 12,000 feet. Lines flown above 12,000 feet demonstrated reasonable internal consistency. The PE_s of these measurements was ± 0.0007 N Mile with the maximum deviation of -0.0020 N Mile.

On 20 August 1963, a flight test was conducted for which the modulation index of the SHIRAN equipment was reduced to approximately 5 radians for experimental purposes. At the reduced modulation index, a slight increase in the noise content of the data was noted. This is borne out by the higher residuals and increased probable error. However, the PE_s of the line, ± 0.0014 N Mile, was still within the specification limit. For optimum system performance, all future operations were conducted with a modulation index of approximately 12 radians.

The overwater tests were repeated 4 and 6 November 1963, at the termination of the Flight Test Program. These results are shown in Table IV. The deviations of nine of the eleven levels of the overwater test flown 4 November were less than $+0.0024$ N Mile. The two large positive deviations fall within a 95 per cent distribution limit.

TABLE IV

RESULTS OF OVERWATER TESTS 4 and 6 NOVEMBER 1963
(Line Gaviota-Point Loma)

<u>LINE NO</u>	<u>ALTITUDE (Feet)</u>	<u>SHIRAN REDUCED (SR) N Miles</u>	<u>V = SR - MEAN SR (x 10⁴) N Miles</u>
<u>4 November 1963</u>			
1	13 671	184 2760	+ 6
2	12 750	184.2763	+ 9
3	11 675	184 2792	+38
4	10 655	184 2736	-18
5	9 640	184 2788	+34
6	8 550	184 2757	+ 3
7	7 495	184 2757	+ 3
8	6 495	184 2736	-18
9	5 500	184 2744	-10
10	4 442	184 2733	-21
11	3 440	184.2730	-24

MEAN SHIRAN = 184.2754 N Miles

$PE_s = \pm 0.0014$ N Mile

TABLE IV (Continued)

RESULTS OF OVERWATER TESTS 4 and 6 NOVEMBER 1963
(Line Gaviota-Point Loma)

<u>LINE NO</u>	<u>ALTITUDE (Feet)</u>	<u>SHIRAN REDUCED (SR) N Miles</u>	<u>V = SR - MEAN SR (x 10⁴) N Miles</u>
<u>6 November 1963</u>			
3	6,050	184.2786	+ 6
4	6 060	184 2786	+ 6
5	6 000	184 2763	-17
6	6 045	184.2786	+ 6
7	7 065	184.2797	+17
8	7 042	184 2789	+ 9
9	7 055	184 2763	-17
11	7 000	184 2794	+14
12	7 100	184 2778	- 2
13	7 050	184.2784	+ 4
14	5 935	184 2770	-10
16	6 040	184 2765	-15

MEAN SHIRAN = 184 2780 N Miles

PE_S = ± 0 0008 N Mile

Geodetic Distance = 184 2766 N Miles (New Mast Location)

The final overwater test performed on 6 November 1963 was flown following standard procedures (two different altitude levels, six crossings in each group). The internal consistency of the results is comparable to overland measurements. The PE_S = ±0.0008 N Mile, the maximum deviation from mean was 0 0017 N Mile, and the difference between the mean SHIRAN length and the geodetic length was 0 0014 N Mile.

2 5 Repeatability Test A second multialtitude experiment was performed between stations Ajo and Catalina. The repeatability test checked the behavior of SHIRAN over rocky and mountainous terrain and over widely varying geometries. Results of this test are given in Table V.

2 5.1 Discussion of SHIRAN Repeatability Measurements.

The repeatability of SHIRAN range measurements was well demonstrated in the Ajo-Cat multialtitude line crossing. The deviations of twenty-one of twenty-eight measurements were less than 0 0010 nautical mile, the PE_S was 0 0006 nautical mile, and the maximum deviation from the mean was 0.0023 nautical mile. The comparison of the final reduced Ajo-Cat distance compared to the geodetic inverse value yielded a difference of 0 0025 nautical

mile An inspection of the various levels in Table V indicates that the overland measurements verified the ability of SHIRAN to measure lines accurately over a wide range of altitudes There was no trend in the measurement errors that could be attributed to multipath.

TABLE V

RESULTS OF REPEATABILITY TESTS
19 SEPTEMBER and 11 OCTOBER 1963
(Line Catalina-Ajo)

<u>LINE NO.</u>	<u>ALTITUDE (Feet)</u>	<u>SHIRAN REDUCED (SR) N Miles</u>	<u>V = SR - MEAN SR (x 10⁴) N. Miles</u>
<u>19 September 1963</u>			
1	11 061	104 6153	+ 5
2	12 044	104 6160	+12
3	13 186	104 6149	+ 1
4	14 234	104 6146	- 2
5	14 234	104.6146	- 2
6	14 234	104 6150	+ 2
7	15 286	104.6128	-20
8	16 361	104 6151	+ 3
9	17 412	104 6146	- 2
10	17 412	104 6152	+ 4
11	18 436	104 6164	+16
12	19 522	104 6152	+ 4
13	20 611	104 6142	- 6
14	22 749	104.6125	-23
15	24 760	104 6159	+11
16	27 001	104 6136	-12
17	30 117	104 6148	0
18	33 201	104.6155	+ 7
19	36 252	104 6147	- 1
20	36 349	104 6147	- 1

MEAN SHIRAN = 104 6148

PE_s = ± 0 0006 N Mile

TABLE V (Continued)

RESULTS OF REPEATABILITY TESTS
19 SEPTEMBER and 11 OCTOBER 1963
 (Line Catalina-Ajo)

<u>LINE NO.</u>	<u>ALTITUDE (Feet)</u>	<u>SHIRAN REDUCED (SR) N. Miles</u>	<u>$V = SR - \text{MEAN SR}$ ($\times 10^4$) N. Miles</u>
11 October 1963			
1	11 084	104.6146	- 2
2	9 992	104.6166	+18
3	8 884	104.6145	- 3
4	7 798	104.6154	+ 6
5	6 747	104.6147	- 1
6	5 676	104.6149	+ 1
7	4 745	104.6142	- 6
8	5 646	104.6147	- 1

$$M = 104.6150$$

MEAN SHIRAN = 104.6148 N. Miles

$PE_s = \pm 0.0006$ N. Mile

Geodetic Distance - 104.6172 N Miles

CUBIC CORPORATION • SAN DIEGO, CALIFORNIA 92123